UNIVERSITY OF CALIFORNIA
RIVERSIDE

Protein-Based Disk Recording for Aerial Densities Beyond 10 Tbit/in.^{2}

A Dissertation submitted in partial satisfaction
of the requirements for the degree of

Doctor of Philosophy

in

Electrical Engineering

by

Matthew Lamar Hudgins

March 2011

Dissertation Committee:
Dr. Sakhrat Khizroev, Chairperson
Dr. Cengiz Ozkan
Dr. Ilya Dumer

The Dissertation of Matthew Lamar Hudgins is approved:

_____

_____

_____

Committee Chairperson

University of California, Riverside

ACKNOWLEDGMENTS

There are many people, whose unwavering commitment, understanding and generosity have made the completion of this work possible. Firstly, I must acknowledge the contributions of my adviser Dr. Sakhrat Khizroev. His guidance and continued passion to execute relevant and ground breaking research has been instrumental in molding my understanding of the applicability of fundamental research toward the resolution of real-world dilemmas.

The text of this dissertation, in part is a reprint of the material as appears in Photo-response of Electrostatically Deposited Bacteriorhodopsin Monolayer Films for Protein-Based Disk Recording Beyond 10 Tbit/in.^{2} J. Nanoelectron. Optoelectron. (In Press) and, Considerations for the Implementation of 2D Protein Based Memory. J. Nanoscience and Nanotechnology (In Press). All co-authors of the aforementioned publications provided technical expertise.

DEDICATION

I dedicate this thesis to my beautiful Fiancé Rebecca. Without her continued support and presence in my life, this milestone would not have been possible.

ABSTRACT OF THE DISSERTATION

Protein-Based Disk Recording for Aerial Densities Beyond 10 Tbit/in.^{2}

by

Matthew Lamar Hudgins

Doctor of Philosophy, Graduate Program in Electrical Engineering
University of California, Riverside March 2011
Dr. Sakhrat Khizroev, Chairperson

Technological developments in the magnetic disk storage industry have relied heavily on the scalability of magnetic bits to ever smaller dimensions in order to provide an increase in areal data densities. This progress has recently been stifled by the Superparamagnetic limit. The Superparamagnetic limit fundamentally restricts the size to which a magnetic bit can be decreased. This limit results from thermal instability of magnetic bits which result in randomization of the magnetic moments within the magnetic media itself as bit dimensions are decreased.

Presently, the Superparamagnetic limit promises to stifle further progress in the magnetic disk-based data storage industry. Therefore, new avenues for technological development in this sector must be pursued to maintain compliance with moor's law and propel future development in this sector at a pace which will keep the industry vital in the coming decades.

In this thesis, a new methodology is proposed by which the technological developments of the traditional magnetic data storage industry can be utilized and the pitfalls of magnetic storage can be avoided. Herein a disk storage implementation involving photo-reactive protein films consisting of Bacteriorhodopsin is presented for extending aerial densities beyond 10 Tbit/in.^{2} System requirements of a commercial application utilizing this technology are presented in detail. The absorption properties of Bacteriorhodopsin (BR) monolayer films, deposited via Electrostatic Self-Assembly, have been studied for the first time to better understand the underlying read/write processes as applicable to this new technology.

TABLE OF CONTENTS

LIST OF FIGURES

CHAPTER I: Magnetic Disk Storage

1. Commercial Development of the Hard Disk Drive

Magnetic disk-based data storage devices have undergone drastic technological advancement over the past six decades. The first practical implementation began with the introduction of IBM's RAMAC computer. The RAMAC contained a hard disk drive with an aerial density of 2000 bits/in^2 and which required fifty 24-inch diameter platters to attain a data density of 4.4MB. Currently hard disk capacities exceed two terabytes and require only two 2.5-inch diameter platters, thereby providing for a 300,000 fold increase in data storage capacity. Additionally, the RAMAC came with a price tag of $50,000, where as current hard drives now can be purchased well under $200 [1]. Power consumption as decreased drastically as well. The RAMAC used 5000W while current HDDs use only 2W.

The drastic increase in areal densities has resulted in a wide array of developments in other consumer product markets including gaming, home theater and portable electronics.

2. Magnetic Disk Storage Fundamentals

Hard disk drives consist of magnetic films magnetron-sputter deposited onto platters. These magnetic films are comprised of grains of the deposited magnetic material [Figure 1].

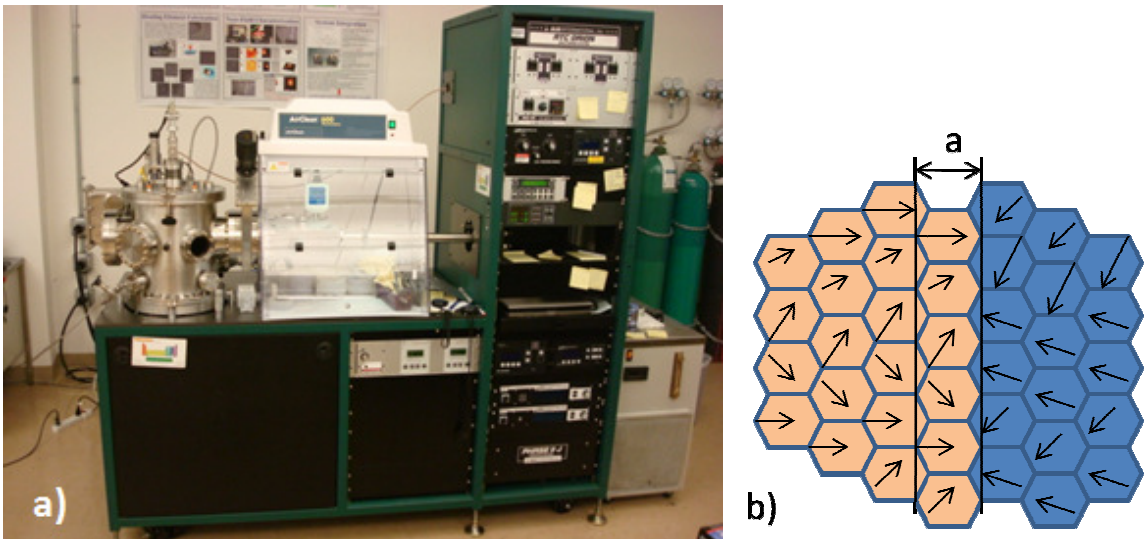

Figure 1: a) Image of a Magnetron Sputtering system and b) Schematic of granular magnetic material with grain width “a”.

This deposition method imparts a preferred magnetization direction of the magnetic moments within the material defining the easy axis. The easy axis indicates a preferential North-South orientation and defines a lowest energy configuration with which to reorient the magnetic bit [Figure 2]. This is necessary as sputter deposition alone would result in magnetic bits with random magnetizations in a device dependent upon a consistent magnetization direction as utilized by the read-write head.

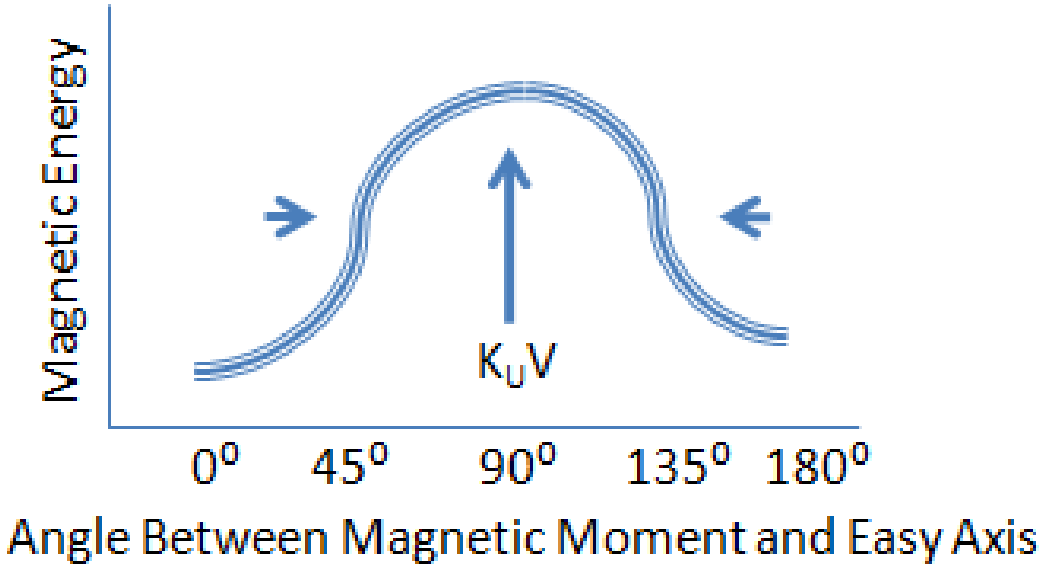

Figure 2: A chart indication the relationship of magnetic energy to the angle between the easy access and the magnetization of the magnetic bit.

Magnetic grains possess a material dependent property called coercivity, which is the energy required to reverse the orientation of a magnetic bit and the coercivity of the material in turn dictates the magnetic field magnitude required by the read-write head to manipulate the magnetic bits within the device. A magnetic bit is comprised of generally between 30 – 80 20nm wide grains which form magnetic domains, where magnetic domains are clusters of coupled grains. The size of the magnetic bit is defined by the dimensions of the read-write head within the device [Figure 3]. Development of higher aerial density media has traditionally involved a reduction of grain volume within a magnetic bit or domain. However, there is a limit as to how small the grains can be made to be, imposed by the Superparamagnetic limit.

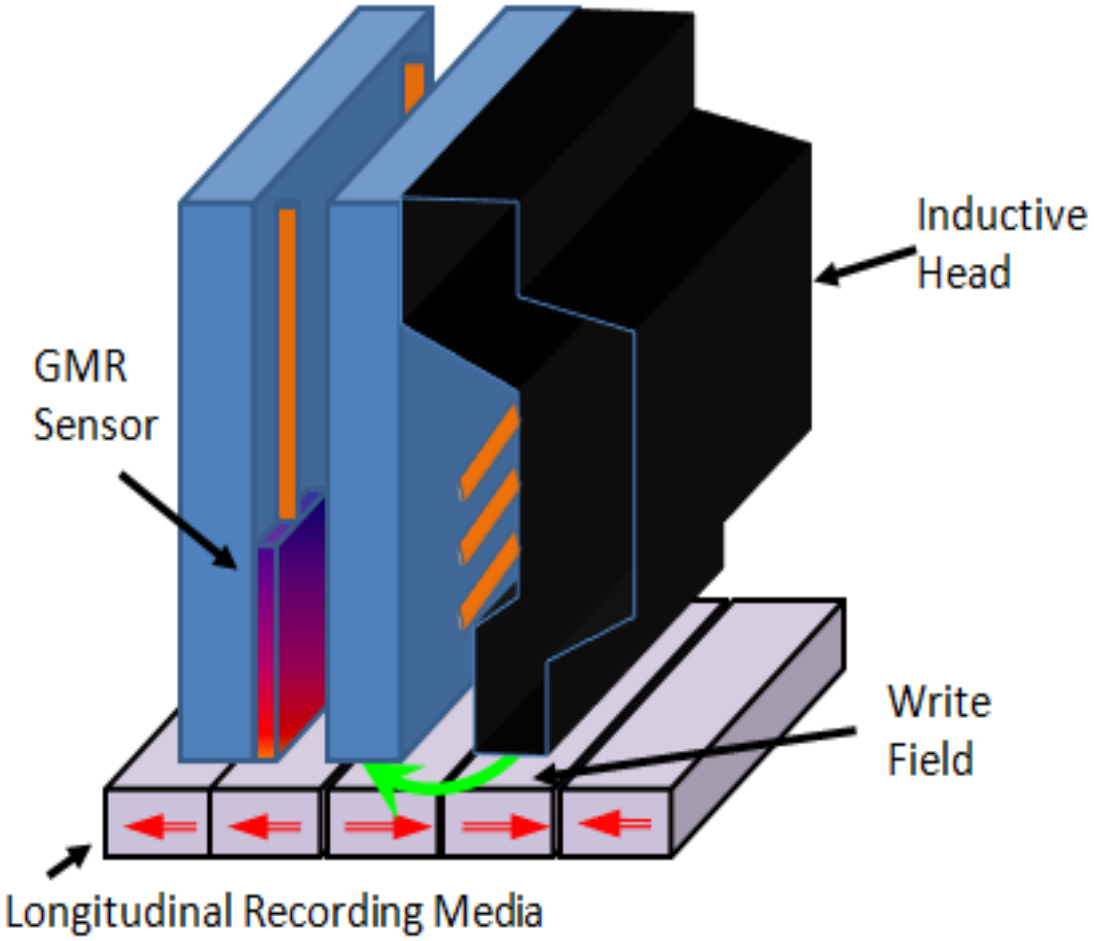

Figure 3: Schematic defining the functionality of a traditional Longitudinal Magnetic Recording device.

3. The Superparamagnetic Limit

The Superparamagnetic limit places a lower bound on the quantity of grains needed to comprise a magnetic bit while still maintaining thermal stability and therefore reliability of the magnetic device [2, 3, and 4]. Quantities below 25 grains per bit reduce the signal to noise ratio (SNR) to a degree such that randomization occurs at room temperature due to coupling effects between adjacent bits. Coupling is a

phenomenon describing the influence that the magnetic fields of adjacent magnetic bits have upon one another. This influence tends to reduce the stability of magnetic materials with a sufficiently low coercivity. As the grain size is reduced, coercivity must be increased in order to maintain predictable operation of the device as thermal effects will further influence the susceptibility of the magnetic bit to randomized reorientation.

The stability of magnetic bits is governed by the following two proportionality relations defining the SNR and t, the thermal activation switching time:

$$SNR \propto \log(K_U V / k_B T)$$

$$t \propto e^{(K_U V / k_B T)}$$

- $K_U V / k_B T = N$ = The Number of Grains per Bit,
- $K_U V = \Delta E$ = Barrier Energy,
- K_U = Anisotropy Energy Density or Coercivity,
- V = Grain Volume, T = Absolute Temperature and
- k_B = Boltzmann's Constant.

Increasing data storage densities typically requires that the quantity or volume of grains be reduced within a magnetic bit, in a process called scaling. The SNR must be preserved while scaling to prohibit thermal instability, which would result in bit randomization. Scaling involves the development of smaller read-write heads and

new magnetic materials for use as thin films with coercivities appropriate to the device requirements. Smaller grains result in thermal instability unless higher coercivity media is used and higher coercivity media necessitates higher applied fields produced by the read-write head. The maximum read-write head field is limited to 2.6 Tesla based on the available materials.

The Superparamagnetic limit imposes a signal-to-noise ratio, thermal stability, and writeability tradeoff that limits the continued scalability of traditional magnetic recording technology to higher storage densities. This Superparamagnetic effect was considered a serious threat to the areal density growth of longitudinal recording technology. This limit has resulted in an industry change from longitudinal magnetic recording to perpendicular magnetic recording. In addition, Heat Assisted Magnetic Recording (HAMR) and Bit Patterned Media have been proposed as possible magnetism based alternatives to propel the development of the traditional Magnetic Based Storage Device [5, 6, 7, 8, 9, 10, 11, 12, and 13].

4. Longitudinal vs. Perpendicular Magnetic Recording

In longitudinal magnetic recording (LMR), the orientation of the magnetic bits are aligned parallel to the surface of the disk [14]. Writing of data is accomplished by the direct influence of the read-write head's magnetic field on the magnetic moment of interest. In perpendicular magnetic recording (PMR) the orientation of the magnetic bits are aligned perpendicularly to the disk however, in PMR writing is

produced by the field in the effective gap [Figure 4] [15, 16]. The effective gap is the region between the trailing pole of the read-write head and the trailing pole of the magnetic image due to the Soft Underlayer (SUL).

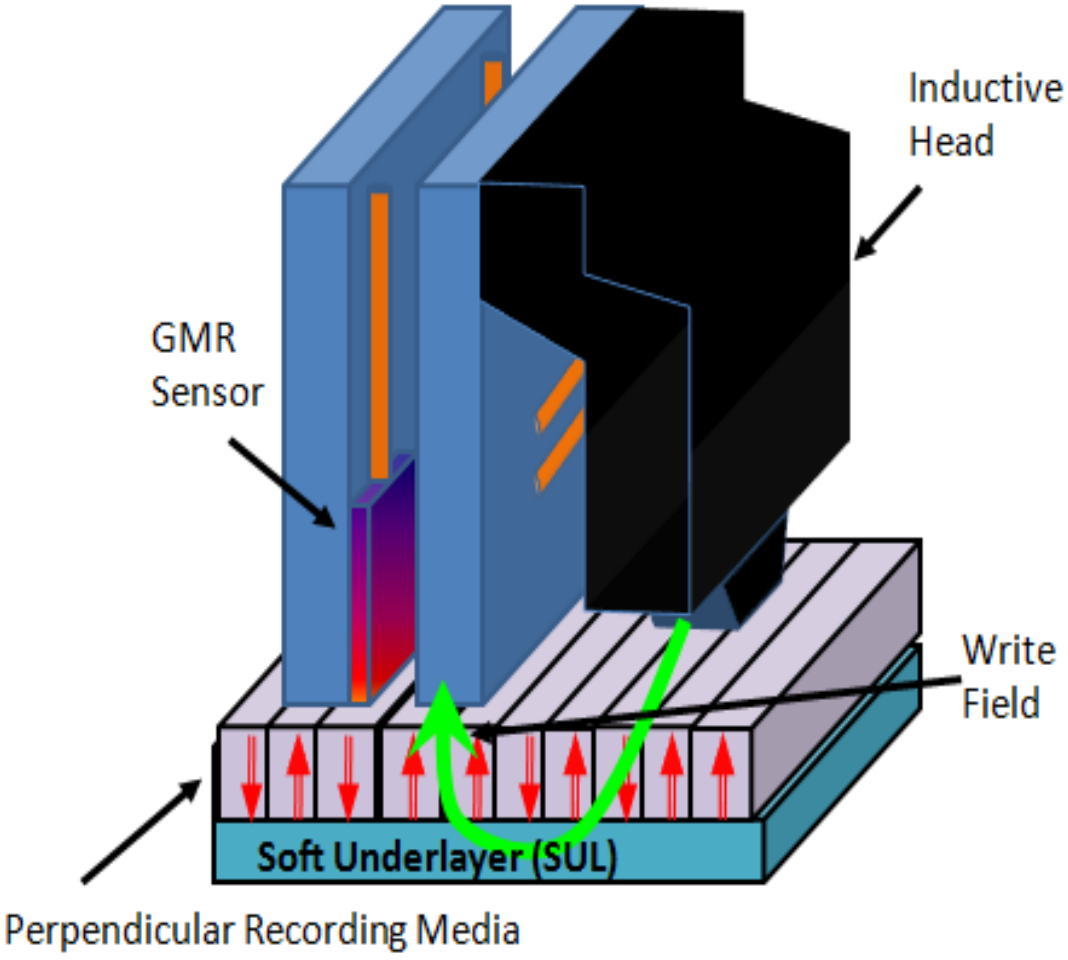

Figure 4: Schematic defining the functionality of Perpendicular Magnetic Recording utilizing a Soft Underlayer (SUL). The magnetic bits are oriented perpendicularly to the media.

The SUL is a layer of soft magnetic material deposited below a layer of hard magnetic material, which is used to image the field provided by the read-write head.

The magnetic image has the effect of increasing the net magnetic field delivered to the magnetic bit and can be considered an extension of the read-write head mechanism. The larger the applied field generated by the read-write head, the larger coercivity material can be utilized as the magnetic media, resulting in an extension of the Superparamagnetic limit.

It is the introduction of SULs in the recording media that provides the significant advantage and development for PMR technology. Higher writing fields can be achieved by using a SUL and a single pole head. Materials with high coercivity can be used as the perpendicular recording media if higher writing fields are achieved. Therefore, smaller grains can be used in the recording medium to store information. This change in orientation of the magnetic media from LMR to PMR has allowed for an extension of the Superparamagnetic limit, increasing data storage densities by a factor of 5 from ~.2Tbits/in^2 to ~1Tbits/in^2.

CHAPTER II: Protein Based Memory

1. Protein Based Memory Overview

Protein-Based devices based on Bacteriorhodopsin were conceptualized in the 1970's. The technology was fervently pursued by the former Soviet Union and their results were kept classified. This was done to compete with western developments in computer technology as an alternative to semiconductor based electronics during

the Cold War. When the former Soviet Union collapsed the research and results they and achieved were destroyed or lost. Their interest in this material and the potential applications thereto has spurred a spate of interest and research by western countries [17, 18, 19, 20, 21, and 22].

Protein-Based Memory (PBM) circumvents all limitations imposed upon magnetic media as read/write schemes utilize optically induced transitions between states called photostates. These photostates are inherent in the protein Bacteriorhodopsin (BR) as the BR photocycle comprises a myriad of photostates with applications in long term and short term data storage devices [23]. With this implementation aerial densities can be extended beyond the current ~1TB/in^2 limitation in PMR to beyond ~10TB/in^2.

Bacteriorhodopsin (BR) is a photo-reactive protein found in Halobacterium Salinarum, an archaeon that inhabits oxygen deprived salt marshes and salt lakes [Figure 5]. BR is used to supplement ATP production in the archaeon when oxygen is not readily available in nature in sustainable quantities [24, 25]. The process by which BR converts light energy to chemical energy has been studied extensively and incorporates the use of a retinal chromophore to transport a proton to different locations within the protein upon light absorption [26]. This has lead to the description of BR as a light driven proton pump.

Figure 5: Photograph of salt lakes in Australia. The Purple areas are the result of Bacteriorhodopsin presence. Image Credit: Cheetham Salt Limited.

2. Bacteriorhodopsin and the Photocycle

The location, to which the proton within BR is transported, depends on the wavelength of light absorbed by the protein [27, 28, 29, 30 and 31]. This process is described by the branched photocycle model which describes the proteins reaction to light as photochromic state changes are induced [30, 32, 33, 34, and 35]. This phenomenon is depicted in Figure 6, where the colored arrows indicate the transitions between the respective states through photochemically induced transitions. The color of each arrow represents the excitation frequency.

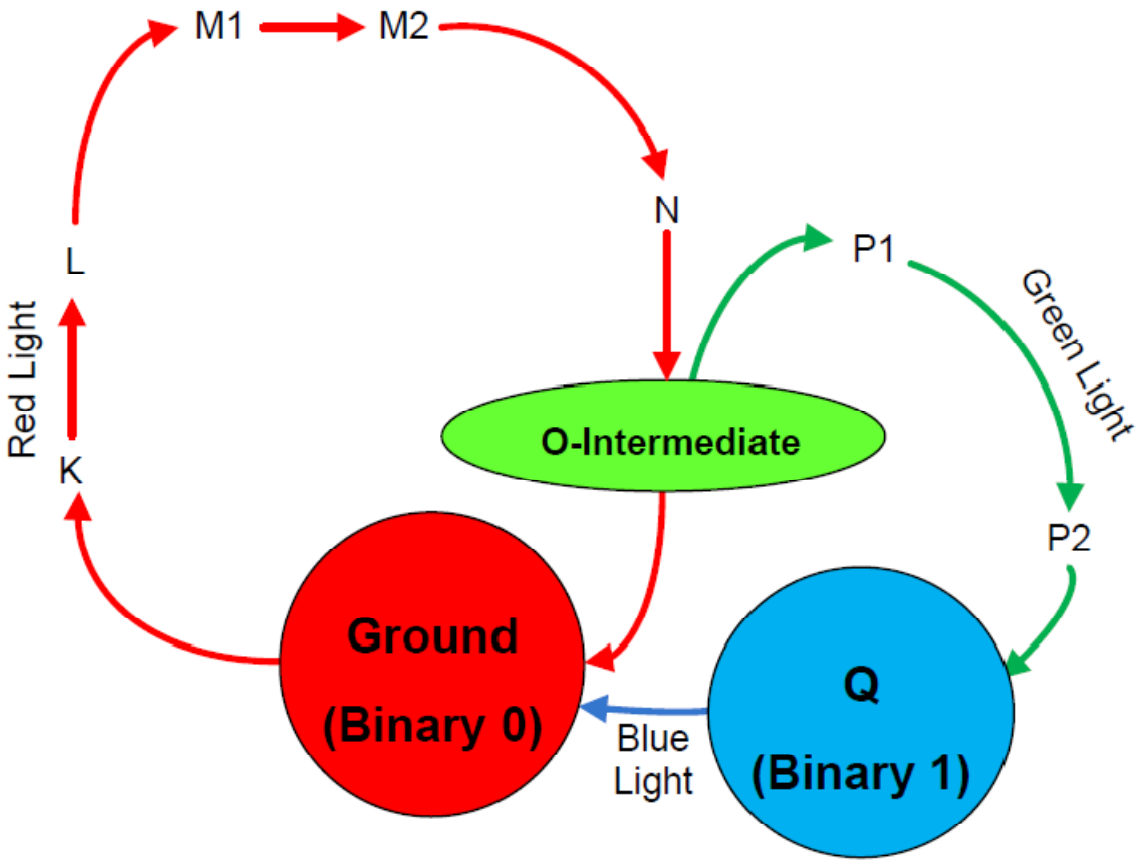

Figure 6: Simplified schematic of the BR Photocycle indicating key photostates suitable for a long term data storage PBM device. (Ground→ O-Intermediate →Q-state). Various intermediate states are shown for reference.

As the photocycle progresses the protein is made to undergo conformal changes resulting in irreversible proton transport, which is believed to be the source of the proteins stability [Figure 7] [36, 37, 38, 39, 40, 41, 42 and 43]. It is this stability that has made protein based memory a possibility. Furthermore, the high cyclicity and high quantum efficiency of BR make this protein an ideal material for use in a PBM device [32, 44, and 45].

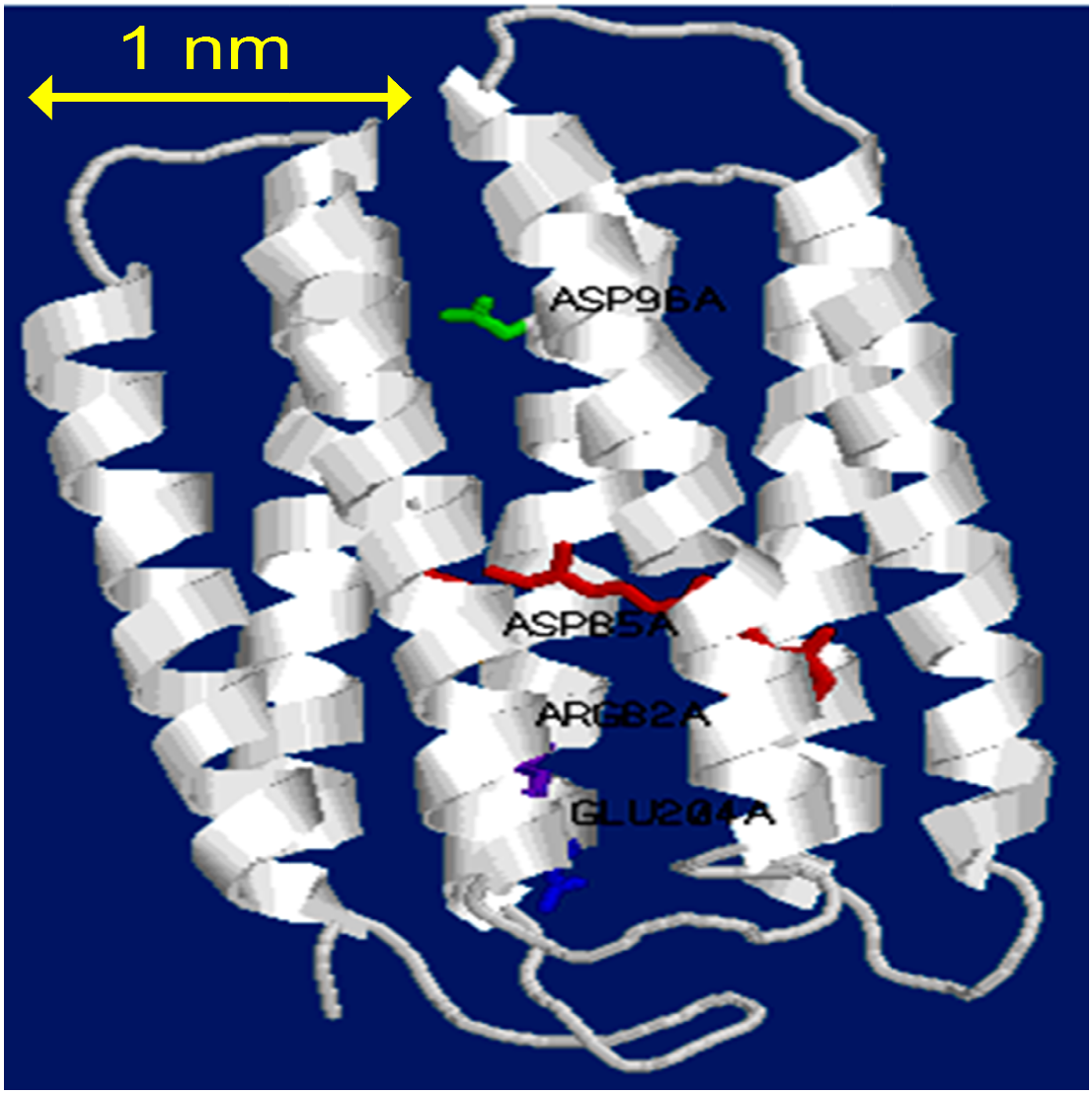

Figure 7: Three-dimensional structure of the BR molecule.

Cyclicity describes the ability of a photoreactive protein to be converted between two different photostates before 37% (1/e) of the material is deprived of its natural properties. The cyclicity of BR exceeds 10^6 at ambient temperature and results from the protective features of the protein membrane [45, 46, and 47]. Quantum efficiency describes the percentage of photons incident on a photoreactive structure

which result in the desired photoresponse. In this case the desired photoresponse is the transition of the proton to different photostates within the photocycle. The quantum efficiency for BR is ~60%, requiring only two photons to induce a photochromic transition between photostates [Figure 8] [48].

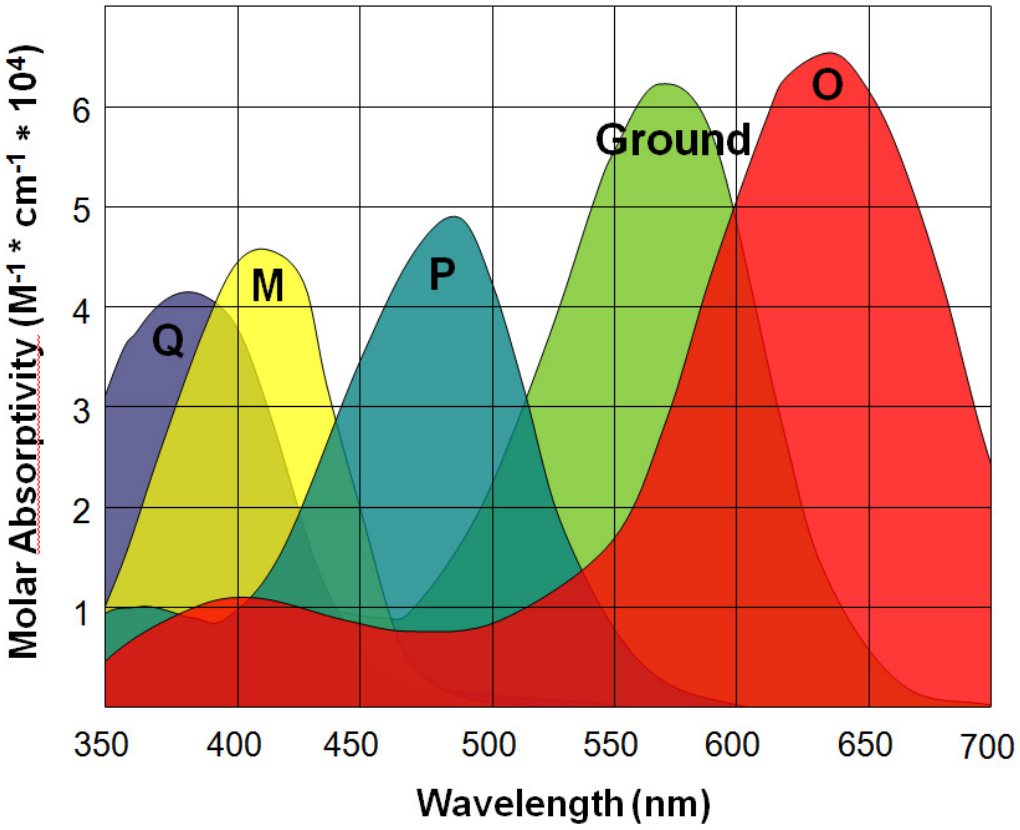

Figure 8: Schematic illustrating typical absorption spectra of the five key states, bR, M, O, P, and Q, in the photocycle of BR.

3. 3D Protein Based Memory

Traditional studies of BR for memory based applications have focused on its uses in 3D volumetric memory [46, 49, 50, 51, and 52]. This type of memory exploits photoelectric signals generated by BR which are indicative of the photochromic

state of the protein [49]. In 3D PBM the material is isolated from the archaeon and refined until only Purple Membrane (PM) remains. The PM containing BR is suspended in optical-grade gelatin. Polyacrylamide cuvetts are used to reduce spectral limitations imposed by other materials [46].

The 3D PBM device implementation involves a two photon write process utilizing two perpendicular excitation sources. The media can be locally targeted via lasers or one source can be used to page the bulk material while the second source locally changes the bit of interest [Figure 9]. This is possible because the photoresponse of BR is specific to the excitation wavelength of light used. In both methods, the initial write source utilizes red light to excite the material to the O-Intermediate state, which has a lifetime of only 7ms. This state will only respond to a subsequent excitation by green light, which propels the media into the Q-state. If no such excitation occurs the protein will revert via thermal transitions back to the ground state.

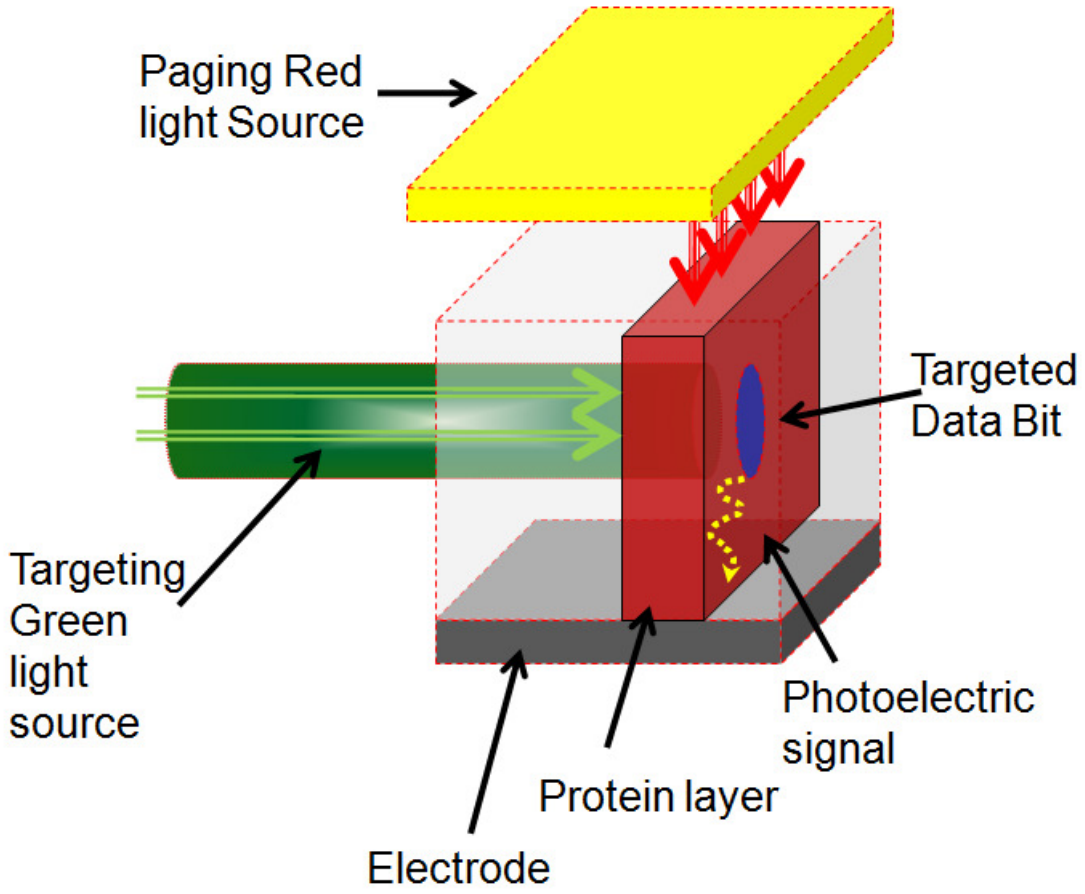

Figure 9: Schematic of the paging write method for 3D Protein Based Memory.

The bit is erased by exposure to blue light which reverts the protein to the ground state from the Q-State. The state of the material is determined by the photoelectric signal emitted from the protein during transitions within the photocycle. This requires the incorporation of an electrode in the PBM device to detect the emitted photoelectric signal.

Unfortunately, this method suffers from beam steering diffraction effects and the inverse relationship of photoelectric signal to electrode distance resulting in dimensional limitations placed upon the media restricting data densities far below current industry capabilities with Magnetic based disk media [46, 49, 50, 51, 52, 53].

4. 2D Protein Based Memory Overview

A device based upon 2D PBM accesses the surface area of a BR coated substrate rather than the volume [Figure 10]. This eliminates the need to compensate for changes in the index of refraction throughout the volume of the media.

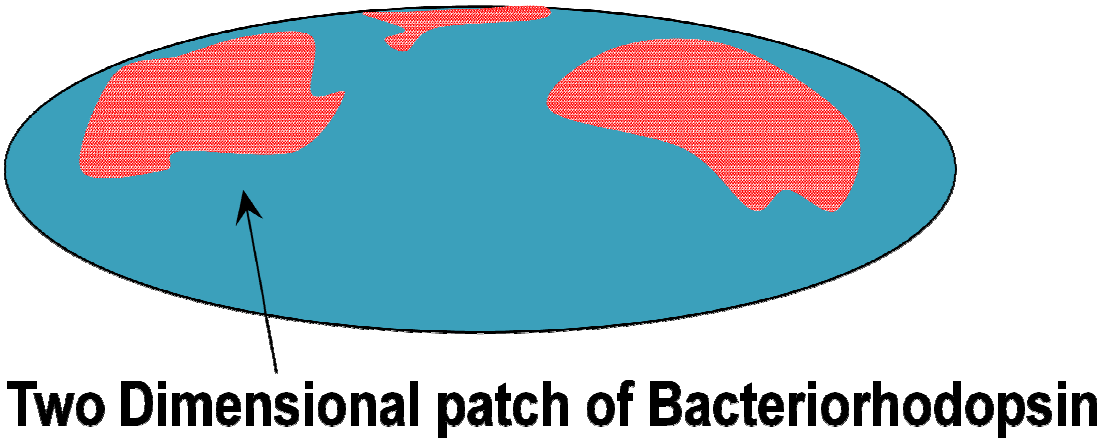

Figure 10: Schematic of a halobacterial cell covered with patches of self-assembled two-dimensional (2D) patches of bacteriorhodopsin.

With 2D PMB, PM patches are deposited on a transparent substrate. Bits are accessed via a read/ write head hovering over the surface, as with magnetic based disk storage devices. The device structure is drastically simplified as compared to the 3D implementation, reducing costs for real – world device implementation. In

addition, there are no beam steering diffraction effects and no self-imposed data density limitations.

A 2D PBM device is functionally similar to the magnetic disk storage device, these similarities allow for the use of data servo methods to track the location of data bits. The device incorporates the near field detection and transmission capabilities of the Near-field Scanning Optical Microscope (NSOM) [Figure 11]. Reading through absorption measurements is possible because the ground and Q-states have drastically dissimilar absorption maxima.

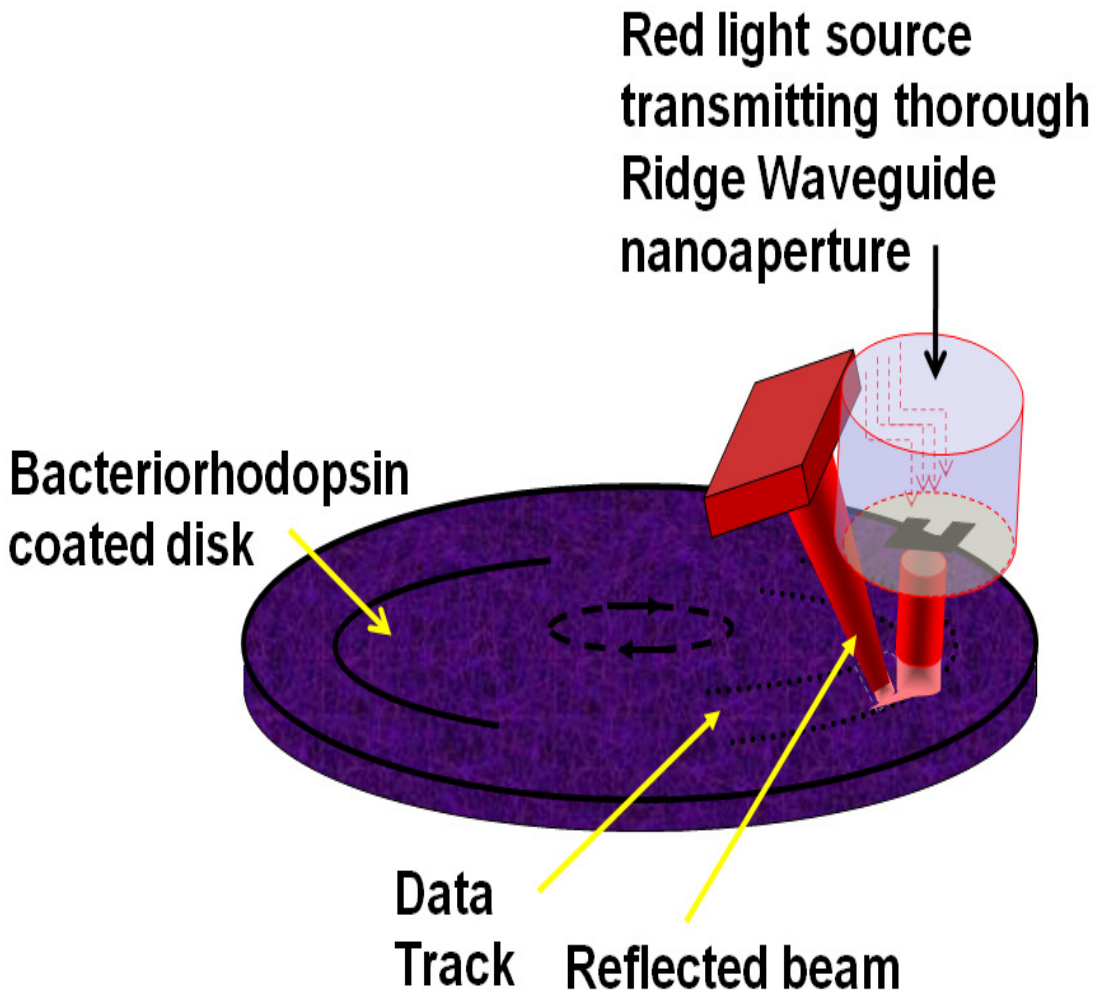

Figure 11: Schematic of a protein disk recording system with signal detection in the reflection mode.

We have proposed the use of semiconductor laser diodes in combination with nano-aperture read/write heads as an initial device implementation [Figure 12]. This method would utilize technology already developed and used in hard disk drives providing a further reduction in cost to implement a commercial PBM based device.

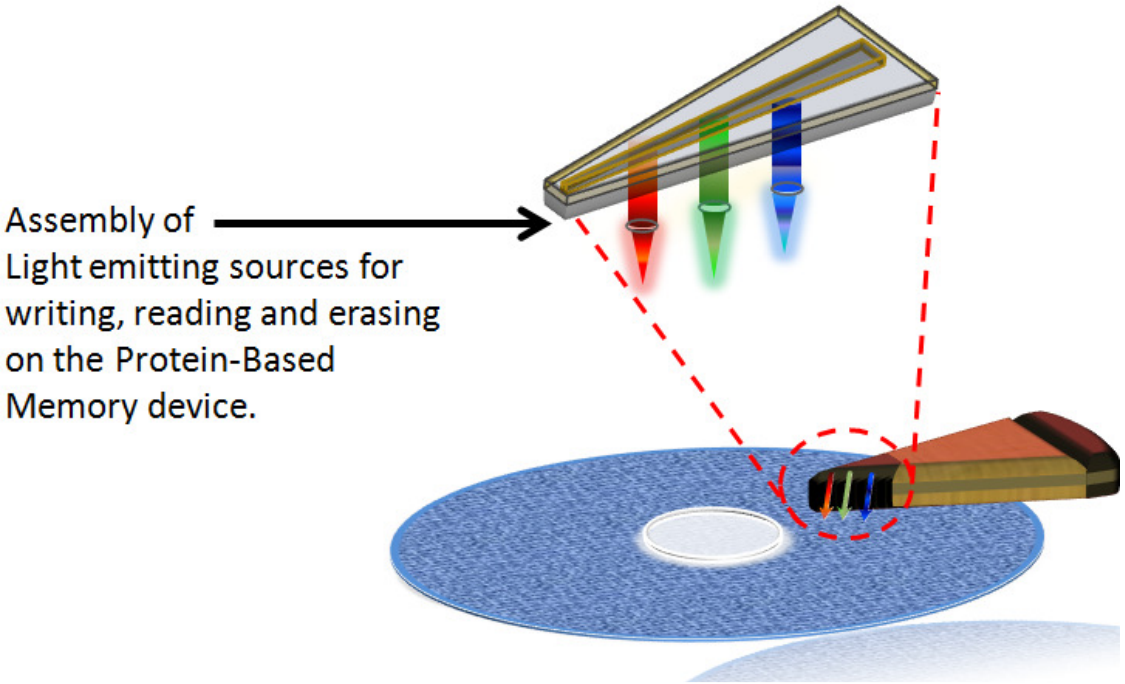

Figure 12: Schematic of a nanoaperture read-write head using semiconductor laser diodes.

Our group has already completed a study to determine the optimal waveguide geometry, which will promote the highest efficiency light transmission for red light. This study entailed FIB etching of an aluminum film which was made to coat the emitting edge of a diode laser [Figure 13] [54]. It was determined that a C – shape aperture or ridge waveguide provided the highest efficiency light transmission on a 30-nm spot. The spot size will determine the data density of the storage media.

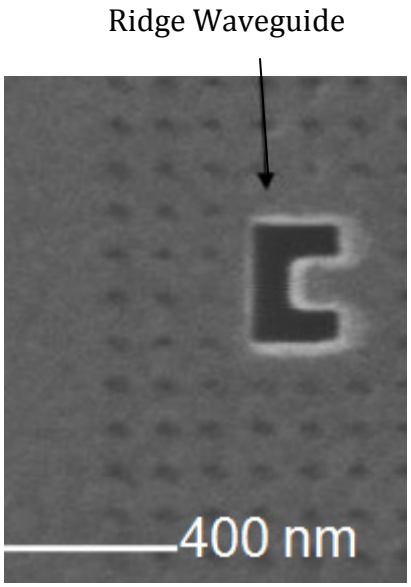

Figure 13: An Ion image of a Ridge Waveguide created via focused ion beam milling on the emitting edge of a diode laser.

CHAPTER III: Protein Thin-Film Deposition Methods

1. Spin Coating

One method considered for the deposition of BR for 2D PBM is spin coating, which involves pipetting an aqueous solution of BR in the form of PM mixed with an optical grade gelatin onto a rotating substrate in a process identical to that which is employed in photolithography [Figure 14]. Excess material is thrown from the rotating substrate as it is spread uniformly over the surface. This process is not an ideal deposition method however, because it does not result in the deposition of monolayer BR PM sheets. In addition, this process wastes a lot of the expensive BR material and requires over 10 hours of dry time so that the gelatin solidifies.

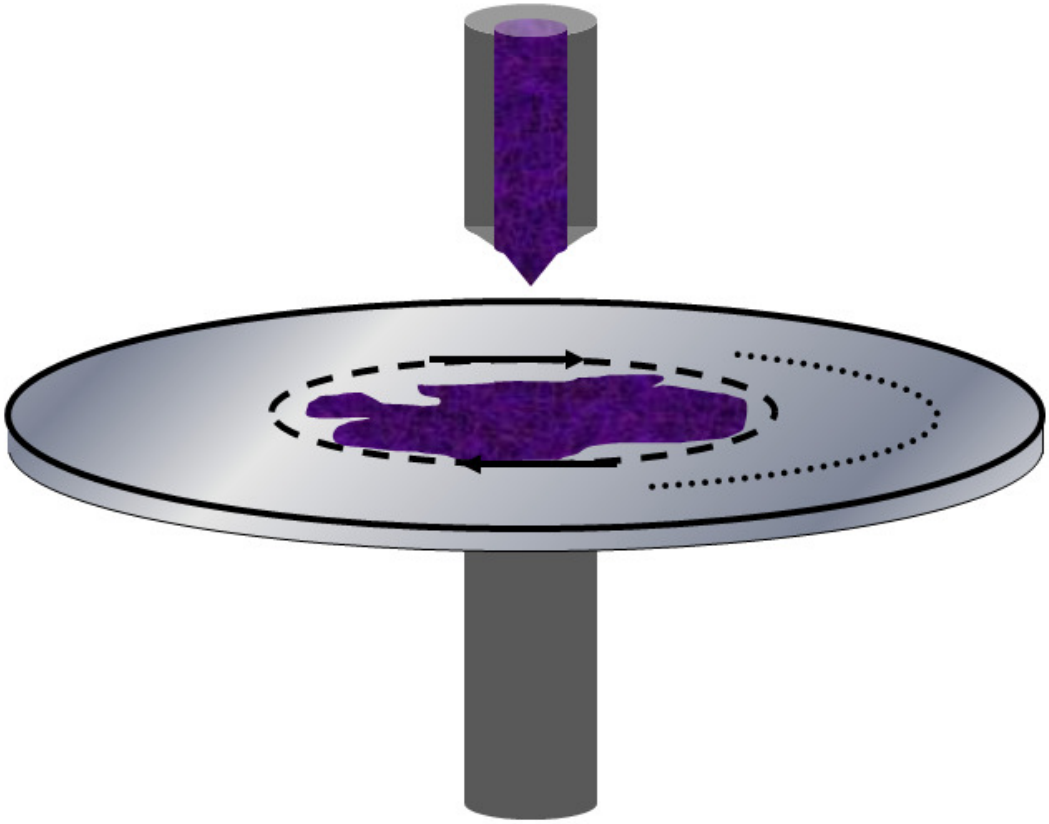

Figure 14: Schematic illustrating the Spin Coat deposition method of BR on a rotating substrate.

2. The Langmuir-Blodgett Technique

The Langmuir-Blodgett (LB) process is a dip coating technique utilizing surface tension to deposit oil based or hydrophobic materials on a substrates surface. The apparatus consists of a DI-water bath kept at constant surface pressure to ensure even uniform coatings of the material are deposited [Figure 15]. The pressure is maintained by mobile barriers within the bath, which move to compensate for the removal of surface material as the substrate is slowly dipped into and removed from

the bath. This process requires a very expensive LB-system and large quantities of expensive BR material.

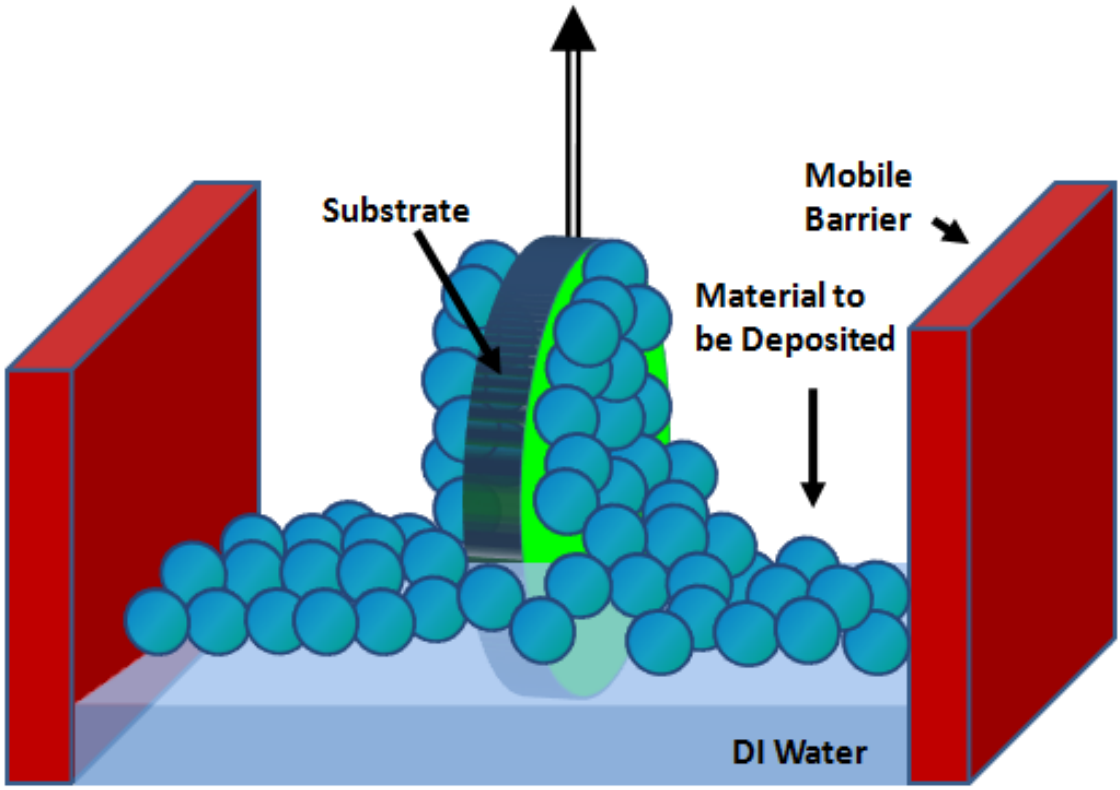

Figure 15: Schematic representing the Langmuir-Blodgett deposition method. The substrate is submerged in a water bath kept at constant surface pressure via mobile barriers. As the substrate moves in and out of the bath, the thin film materials lying on the top of the bath are deposited.

Deposition of BR material using this method involves the suspension of BR in a hexane solution consisting of L-alpha-phosphatidylcholine (soya-PC) and basal salt. A micro-syringe is used to coat the surface of the DI water bath with the prepared solution. The material is hydrophobic ensuring the material remains on the baths surface and the initial surface pressure is allowed to stabilize at 40.0mN/m. The subsequent dip coating process requires precise control of the barrier speed

maintaining the surface pressure and the insertion and extraction rates of the substrate in the bath. The substrate is allowed to dry for 45 minutes to promote adhesion. This process allows for the deposition of a thin coating of the BR and soya-PC material to the substrate, however the process does not ensure the deposition of monolayer BR.

3. Electrostatic Self-Assembly

BR in the form of PM is an inherently anionic material, which can be exploited to employ the use of Electrostatic Self-Assembly (ESA). The method employs the use of electrostatic charges to bind together oppositely charged materials [Figure 16] [55, 56]. Processes utilizing silicon based supports, such as quartz, glass and silicon wafers typically involve imparting upon it a net negative charge via hydrolysis of the surface with a basic solution. Materials are deposited via submersion of the charged substrate into oppositely charged aqueous solutions until the desired material composition is achieved.

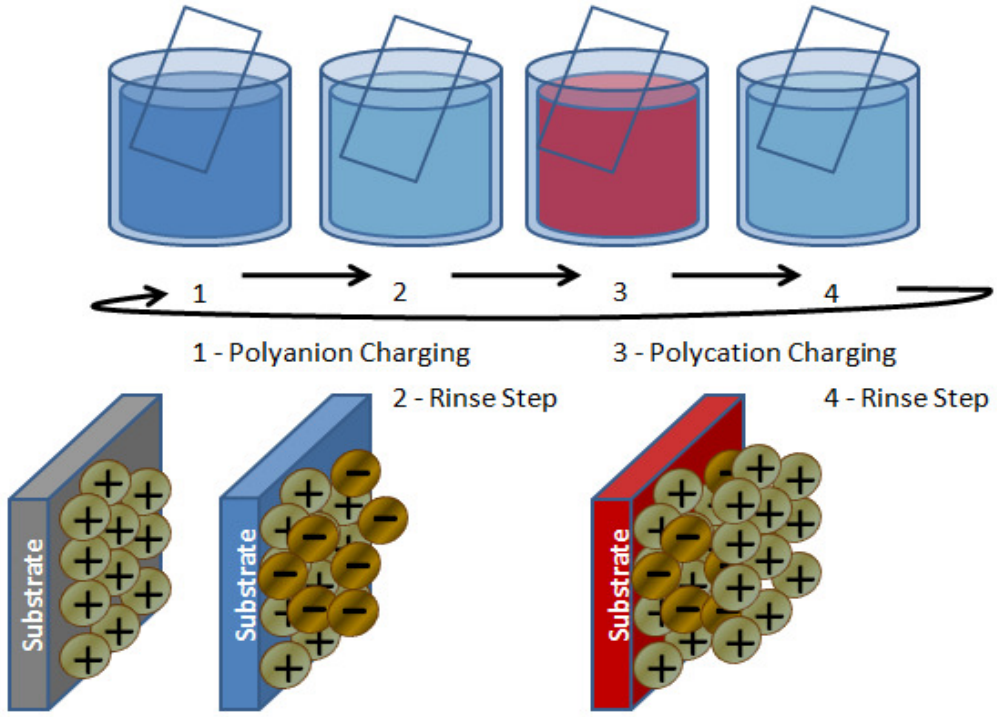

Figure 16: Schematic of the Electrostatic Self Assembly material deposition technique. A positively charged substrate is submerged in an anionic solution followed by a rinse step to remove excess material. The now negatively charged substrate is submerged in a cationic solution of the desired deposition material followed by a rinse step. The method can be repeated to deposit more bilayers.

Deposition of BR using ESA involves the submersion of Glass or quartz slides in a basic solution, typically KOH. The basic solution removes protons from the substrates surface imparting upon it a net negative surface charge. The charged substrate is then submerged in Poly(diallyldimethylammonium chloride) (PDAC) of medium molecular weight. PDAC is a cationic intermediate layer and does not absorb light in the visible spectrum. This step yields a net positive charge on the substrate. The now positively charged PDAC bearing substrate is submerged in an aqueous PM solution. The anionic BR in the form of PM fragments adheres to the surface.

For our purposes ESA is the most practical as it allows for the deposition of monolayer films and it's an inexpensive and highly reliable process. There is no large equipment required and the necessary infrastructure is present in the UCR cleanroom. It is for these reasons that ESA is the deposition method of choice for use in creating a 2D PBM device.

CHAPTER IV: Spectral analysis of BR Monolayer Films

1. Deposition of Poly(diallyldimethylammonium chloride) (PDAC)

This section addresses the use of Poly(diallyldimethylammonium chloride) (PDAC) in conjunction with electrostatic self assembly (ESA), for the production of an ultrathin cationic seed layer to be used in novel memory devices. In this way, proteins and other materials with an inherent negative charge, or those materials that have been functionalized to bear a net negative charge can be used for ESA based deposition onto a prepared cationic PDAC layer. The importance of this method lies with an inherent problem faced in the advancement of traditional hard drive based magnetic storage devices, the Superparamagnetic limit.

The Superparamagnetic limit places a fundamental limit on the grain size of magnetic domains in a magnetic storage device, due to increased interference effects between magnetic bits as bit size is reduced in pursuit of higher aerial storage densities. It has been proposed by our group that the use of certain anionic

proteins could circumvent this limit altogether, allowing for devices with aerial densities of up to 10 Terabits/in2. To that end, PDAC has been explored as an intermediate layer to be used between a negatively charged substrate and an anionic protein layer.

Gold crosses were formed on a cleaned silicon substrate using standard photolithographic techniques so that step height measurements could be taken to determine the deposition rate of PDAC material. Photoresist was spin coated onto the substrate, hard baked and with the use of a mask and UV light the crosses pattern was superimposed upon the substrate. 3D cross shapes were formed by chemical etching of the unexposed photoresist material from the samples surface. A layer of Gold 35nm thick was deposited by Electron-beam evaporation across the entire substrate. The excess gold material was removed by submersion in Acetone resulting in the creation of gold crosses [Figure 17].

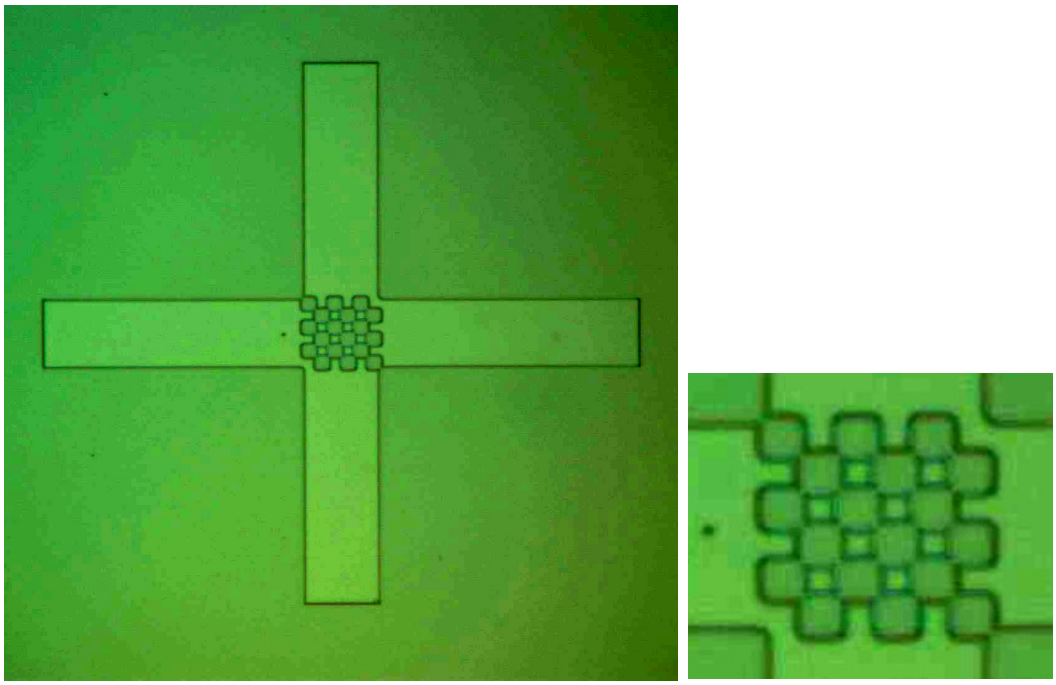

Figure 17: An optical image of a lithographically imposed gold cross pattern used to enable stepheight measurements for PDAC thickness determination.

Substrates were cleaned thoroughly again in Ethanol/Chloroform/Acetone (2v/v/v). The cleaned gold cross samples were submerged in a solution of 2% KOH in DI water to impart a net negative charge upon the surface silicon oxide layer. The cleaned substrates now bear a net negative charge on the silicon oxide layer surface and not the gold surface.

The negatively charged silicon substrates were submerged in the positively charged PDAC solution for 5 minutes resulting in the adsorption of 10nm of PDAC on the substrate. The PDAC layer is deposited on the prepared sample via ESA due to its inherent positive charge which in turn promotes the adsorption of negatively

charged molecules, namely BR. Deposition of PDAC produces an inherently smooth and homogenously coated surface [Figure 18].

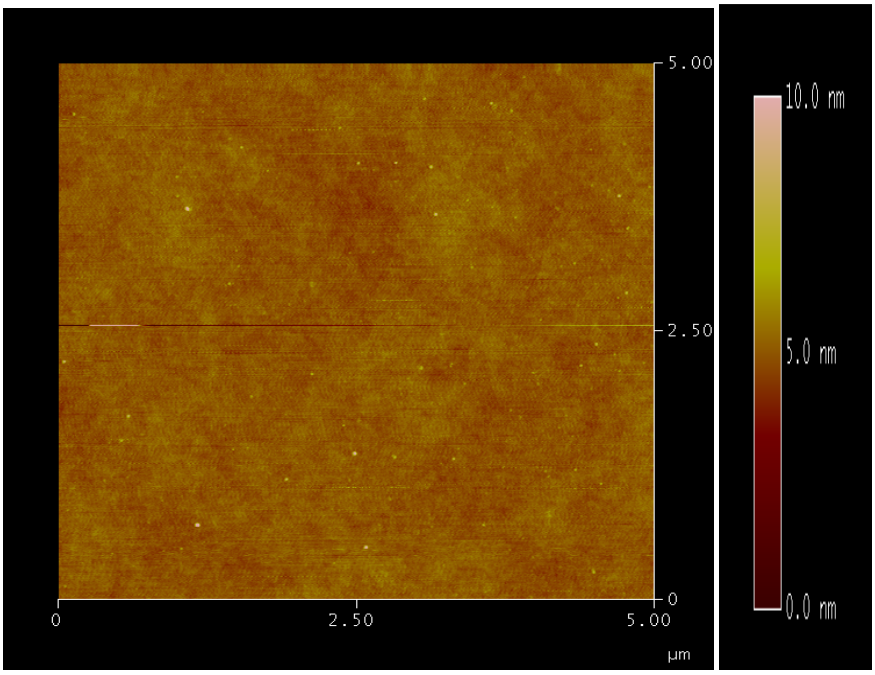

Figure 18: An AFM image of a Silicon substrate coated with a 10nm thick poly(diallyldimethylammonium chloride) (PDAC) thin film.

Atomic Force Microscopy was used to ascertain the thickness and homogeneity of electrostatically deposited PDAC thin films as a function of substrate submersion time on lithographically patterned media. The desirably smooth surface of a PDAC coated sample makes it difficult to characterize via Atomic Force Microscopy (AFM) and necessitates the lithographic patterning process described previously.

In order to accurately determine PDAC thickness as a function of submersion time, several step-height measurements are taken during each process phase [Figure 19].

Measurements are repeated on the same cross after each step for continuity. The reproducibly of this deposition process enables accurate calibration of the BR layer thickness. Fine tuning of the BR layer will be necessary to optimize the absorption characteristics of the resultant device. The stepheight measurement shows the difference in height from the lower silicon surface and the higher gold surface.

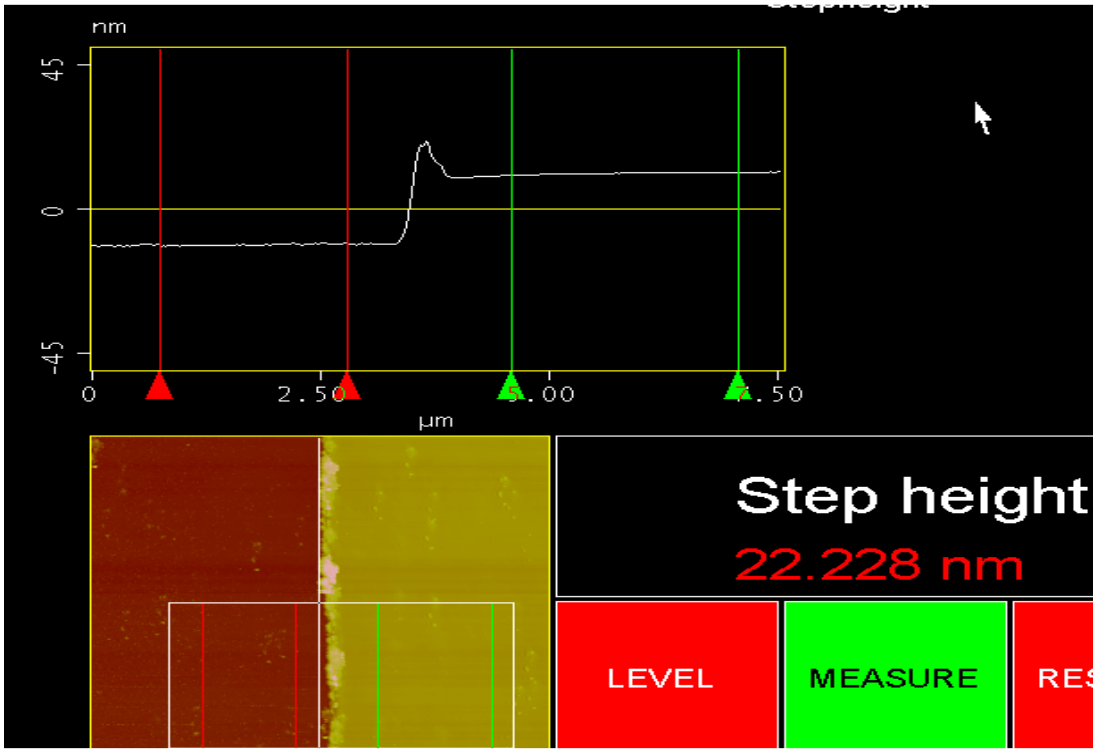

Figure 19: An AFM image of stepheight measurement of poly(diallyldimethylammonium chloride) (PDAC) on a negatively charged silicon substrate with 35nm thick gold crosses lithographically imposed upon the surface.

2. Deposition of Bacteriorhodopsin using Electrostatic Self-Assembly

BR was successfully deposited on glass slides as described in Chapter III, section 5 however, this process yielded large particle clusters on glass [Figure 20].

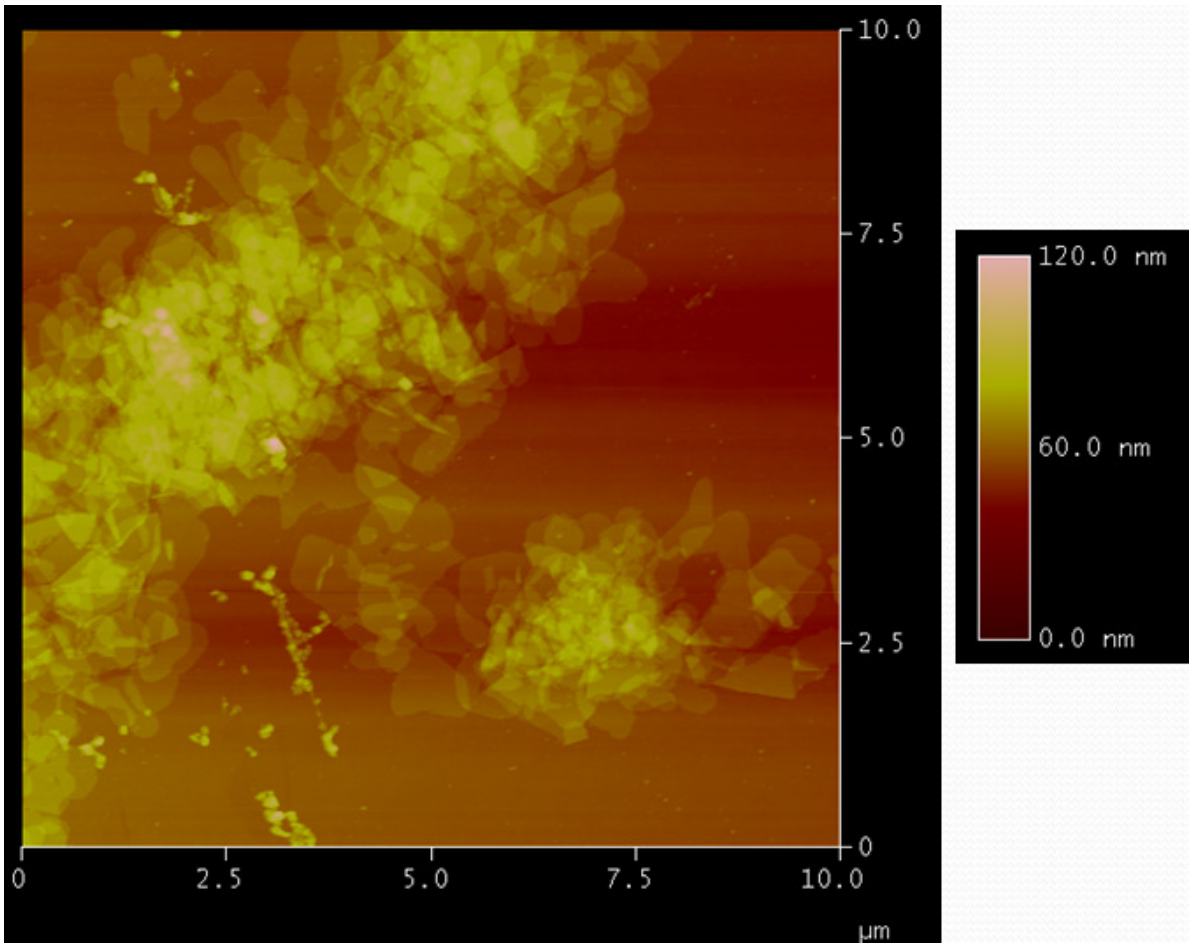

Figure 20: AFM image illustrating the typical result of the deposition of PM on Glass using ESA resulting in the adsorption of large clusters of PM material.

The absorption spectra was taken using a Cary 5000 spectrophotometer and was in good agreement with other with literature for a material deposited using ESA and described as two bilayers of BR / PDAC material [Figure 21] [55]. A characteristic peak at 596nm can be observed in the material.

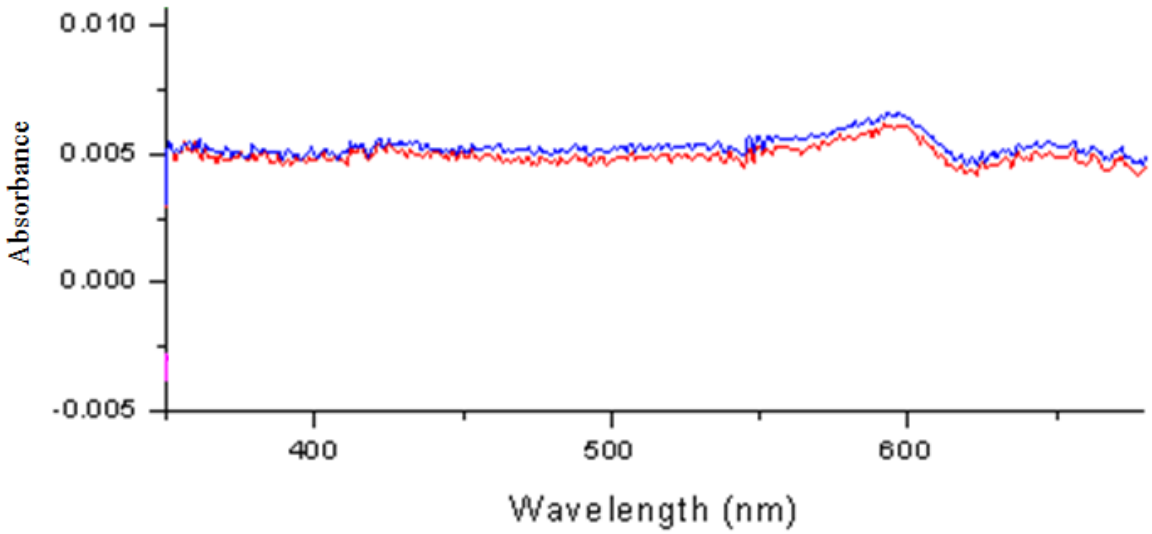

Figure 21: Absorption spectra of large clusters of PM material deposited via electrostatic self assembly on glass using a Cary 5000 Spectrophotometer.

The process was further refined to incorporate sonication during the deposition of BR, thereby promoting the adsorption of single PM sheets and the dissociation of large PM aggregates. Deposition of BR during sonication was found to significantly reduce adsorption of large PM clusters [Figures 22 and 23]. Large clusters were mobilized such that they were able to overcome the coulombic interactions between the charged substrate and the BR material in solution. Only monolayer patches were allowed to adhere to the surface.

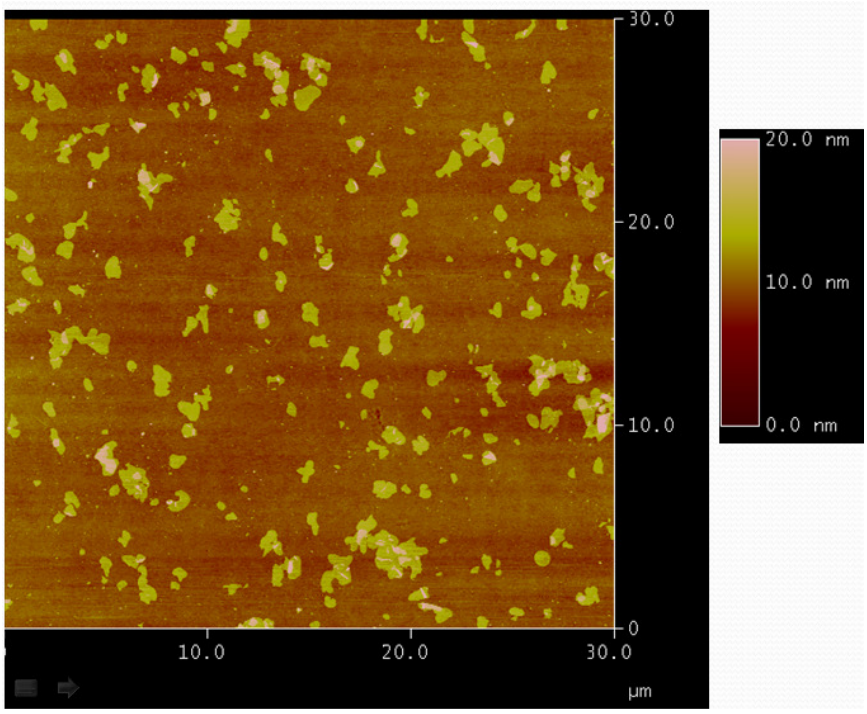

Figure 22: A 30µm AFM image of monolayer BR in the form of PM sheets on Glass deposited via ESA under sonication.

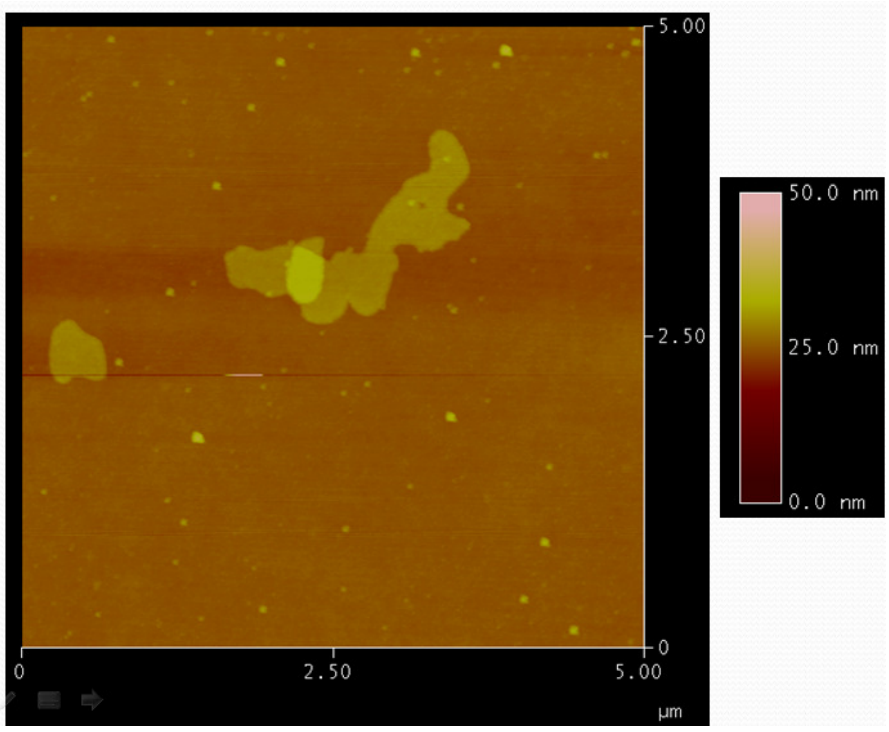

Figure 23: A 5µm AFM image of monolayer BR in the form of PM sheets on Glass deposited via ESA under sonication.

3. Determination of protein surface density

Electrostatically deposited Bacteriorhodopsin films were determined to have an average protein surface density of 12.6% utilizing Matlab for image analysis [Figure 24]. MATLAB (MATrix LABoratory) is a mathematical computation environment which provides additional programming functionality.

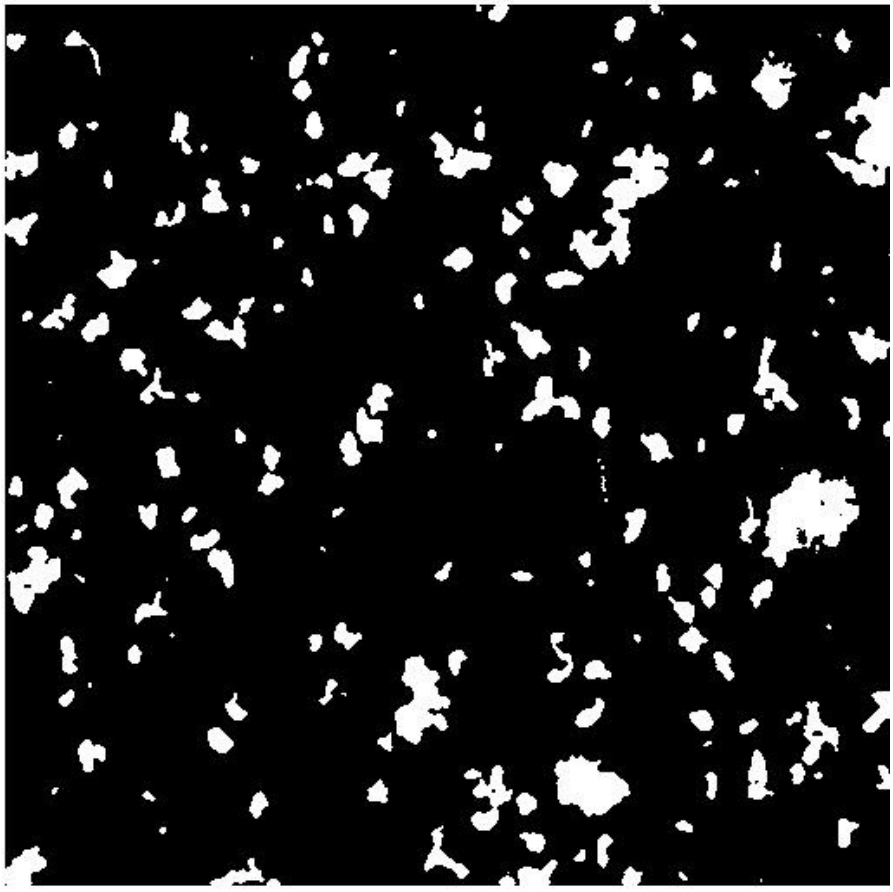

Figure 24: A MATLAB modified AFM JPEG image of monolayer bacteriorhodopsin on glass.

MATLAB allows for JPEG image modification as JPEG images store Red-Green-Blue color information within a series of matrices within the image file. These matrices

were isolated and the image adjusted such that the yellow protein segments of the AFM image were isolated and made to be white while the rest of the image, the non-protein portion or background, was set to black. The additional benefit of this method, when used in combination with AFM images is that the precise height can be isolated. AFM images comprise a color gradient with scale. Isolating a single color within the AFM image isolates an individual slice or level of the sample image ensuring attainment of the homogeneity of the image as used for surface density measurement.

4. Photo-response of Electrostatically Deposited Bacteriorhodopsin Monolayer Films for Protein-Based Disk Recording Beyond 10 Tbit/in.^{2}

a) Introduction

Upon the absorption of a photon, BR undergoes a series of structural changes that convert light energy to chemical energy [26]. This process is described by the ever evolving photocycle model, whereby the reaction of BR to light is explained in terms of a cyclical progression through a series of states with finite lifetimes [30, 32, 33, 35, and 36].

The innate photophysical properties of BR make it a promising material for use in next generation Protein Based Memory (PBM) devices. These properties include high cyclicity, high quantum efficiency and the existence of multiple photochromic

states that prove useful for both long term and short term data storage [32, 45, and 46]. Previous studies of BR based optical memories have focused on its uses in 3D volumetric memory [46, 49, 50, 51, and 52]. This type of memory exploits the photoelectric signals of BR that are indicative of the photochromic state of the protein.[10]

Unfortunately, it has become increasingly apparent that a 3D implementation is not immediately practical, due to the inverse relationship of photoelectric signal to electrode distance resulting in dimensional limitations placed upon the media [46, 49, 50, 51, 52]. This problem is compounded by beam steering diffraction effects, which place restrictions on the ratio of ones to zeros within the volumetric pixel (or voxel) and the proximity of individual bits within the voxel to one another, further decreasing the volume available for data storage [53]. These limitations have thus far restricted the data density of 3D memory far below the theoretical threshold.

Two dimensional (2D) optical memories do not face the same limitations due to the lack of intermediate protein layers. This advantage allows for direct accessibility of the protein storage medium. It is for this reason and the emerging technology of near-field optical transducers [54] that a 2D implementation in the form of Protein-Based disk storage has become a feasible alternative to 3D PBM. Moreover, data storage devices utilizing BR can theoretically extend areal densities of disk based data storage devices beyond 10Tbit/in^2 [48].

Attainment of a traditional binary data storage device with 2D BR films requires that several photostates be used in the photocycle. Accessing these states requires traversing the photocycle in the following sequence: ground (**bR**) state, **O** intermediate, and the **Q** state. In protein-based memories, the **bR** and **Q** states are the two stable photoproducts necessary for binary recording. A binary one is written by exposure of the protein to green light exciting the proton to the **O** intermediate, then red light exciting the protein to the $\mathbf{P_2}$ state, followed by thermal relaxation to the **Q** state [36]. The **Q** state is reverted to **bR** indicating a binary zero, by exposure to blue light.

The **Q** state contains a hydrolyzed 9-cis retinal and has a lifetime of approximately 10 years, which meets current industry standards set for traditional magnetic data storage devices [32]. As a dry film, BR can function at temperatures up to 140^{o}C and pressures up to 300GPa providing unprecedented stability and versatility [57]. The protein also has a quantum efficiency of 65 percent and requires less than 2 photons to induce each data storage event [48]. In this paper we report progress on the material deposition and photo-induced transitions of 2D BR monolayer films.

b) Experiment

Wild-type BR, in the form of purple membrane (PM) powder, and Poly(diallyldimethylammonium chloride) (PDAC, medium molecular weight) a transparent water soluble cationic polymer were purchased from Sigma-Aldrich.

Solid substrates comprised of 1mm thick glass slides. The inherent anionic nature of BR was exploited to employ the use of Electrostatic Self-Assembly (ESA) [55]. The method employs the use of electrostatic charges to bind together oppositely charged materials. Processes utilizing silicon based supports, such as quartz, glass and silicon wafers typically involve imparting upon it a net negative charge via hydrolysis of the surface with a basic solution [55, 56].

Substrates were cleaned in an ultrasonic bath at 25^{o}C for 25 minutes in a solution of ethanol/acetone/chloroform (2v/v/v), charged via submersion into a 2% KOH solution under the same conditions, rinsed with DI water and dried with N_2 gas. The substrates were then submerged in PDAC for 5 minutes at room temperature, rinsed in DI water and dried with N_2 gas. This resulted in the adsorption of a monolayer of PDAC. Next, the substrate was submerged in PM solution for 5 minutes in an ultrasonic bath, rinsed in DI water and dried with N_2 gas.

PDAC/PM coated samples were characterized via Atomic Force Microscopy (AFM). A Cary 5000 spectrometer was used for absorption measurements. An LED device that provided independent control of Red, Green and Blue light was attached to the spectrometers sample holder. The device consists of four red, green and blue LEDs respectively, angled at 45° incident to the back of the sample. This device allowed for direct illumination of the sample before each absorption measurement and

eliminated any ambient light contamination of the protein photochemistry. Samples were illuminated for approximately 5s prior to each measurement. This configuration allowed for an unobstructed path from the spectrometers source in front, to the detector at the rear.

Isolated PM sheets were found to have drastically varied geometries (Figure 25), and were determined to have an average protein surface density of 12.6%. Matlab was used for image analysis. Aggregation of single layer PM sheets was found to improve with the application of an ultrasonic bath during PM deposition. A possible explanation of this improvement is that the energy provided by the ultrasonic bath promoted the mobilization of larger PM fragments in solution due to their larger surface area, which allowed them to overcome the columbic forces experienced between the anionic PM fragments and the cationic PDAC layer previously deposited on the glass substrate. This phenomena effectively promoted the more favorable aggregation of single layer PM sheets. Moreover, the energy provided by the ultrasonic bath promotes the dissociation of PM fragments in solution, yielding higher quantities of monolayer film material available during deposition.

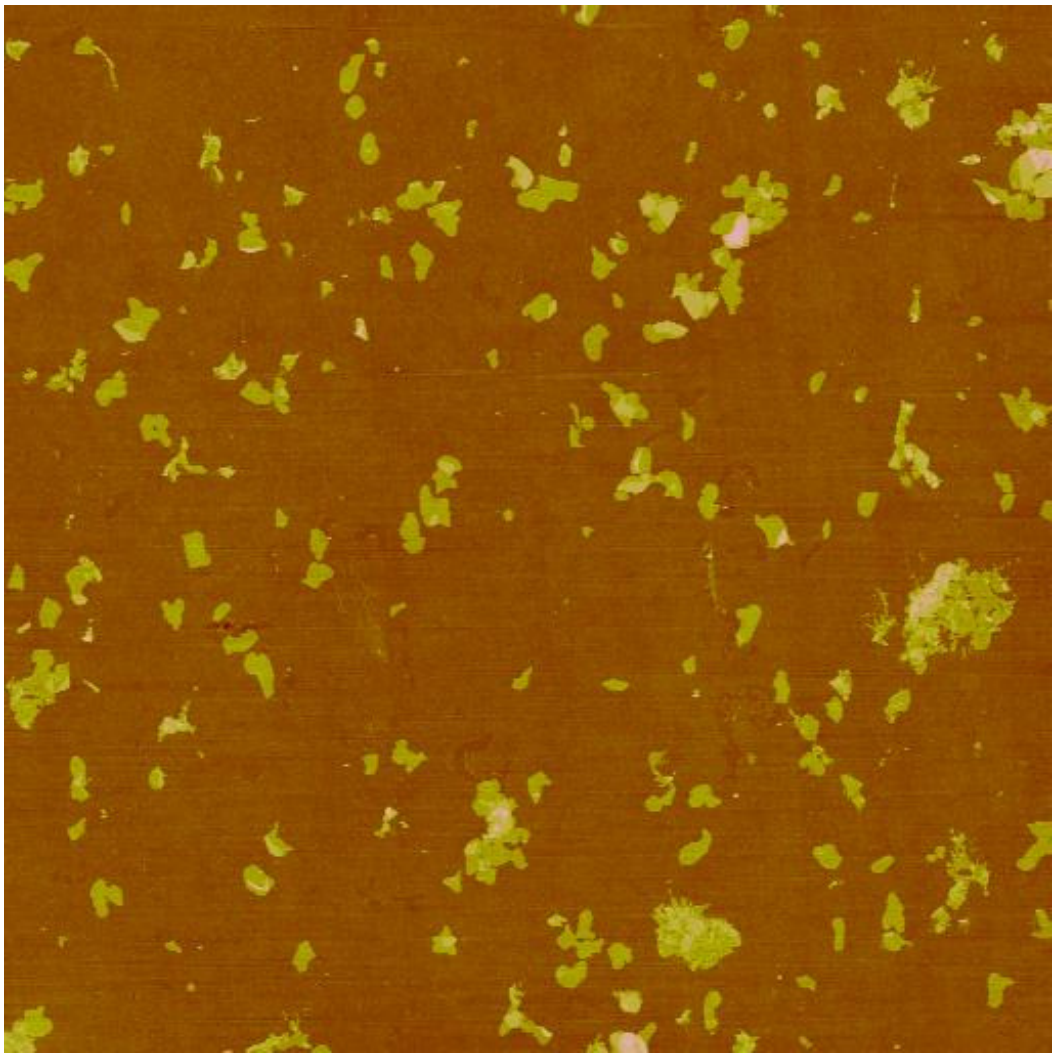

Figure 25: AFM image of monolayer BR in the form of Purple Membrane sheets on glass, deposited via Electrostatic Self Assembly.

The results of absorption measurements taken from 800 to 285 nm of BR monolayer films after LED irradiation are presented in Figure 26. A sharp peak in fluorescence corresponding to pronounced negative absorption occurs below 335nm and occurs independently of external excitation. Furthermore, it was observed that irradiation with blue light results in a marked reduction in absorption

above 430 nm as the protein fluoresces in transition from the **Q** state to the **bR** state. Peak fluorescence was found to occur at 755 nm of magnitude 5.27e-4 in the region above 430 nm. This observation is consistent with results from previous works utilizing volumetric aqueous BR solutions, indicating fluorescence maxima occur in BR between 700 and 790 nm [58, 59, 60, 61, 62, 63, 64, 65, 66, 67, 68, 69, and 70].

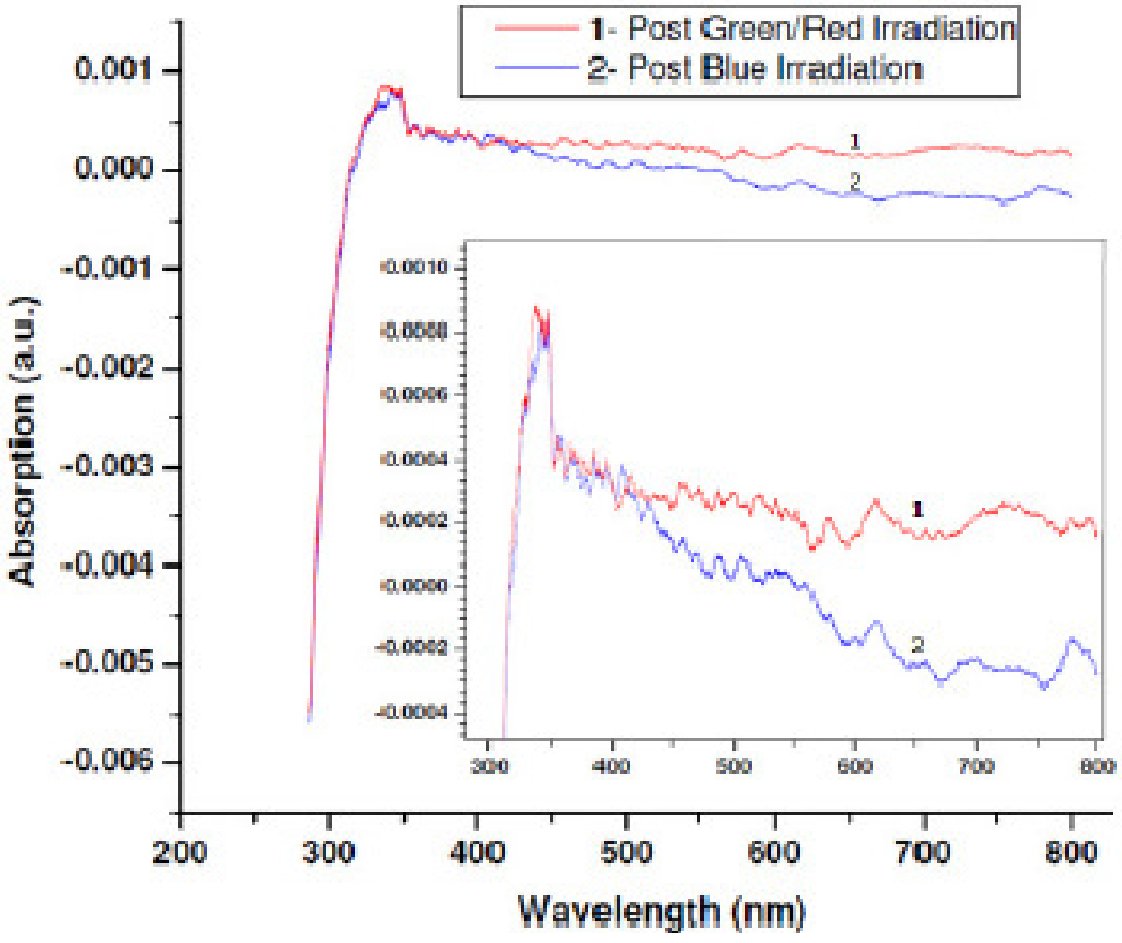

Figure 26: Absorption spectra of BR monolayer film after irradiation with Green / Red and Blue light.

Our observed absorption spectra of BR monolayer films are believed to result from decreased mobility of the BR proton due to columbic interactions between the substrate and protein. This interaction results in a maximum difference of 5.27e-4 in BR at 755 nm, between the **bR** and **Q** states. Previous studies focusing on aqueous BR solutions utilize proteins that are not subject to the same confinement.

c) Conclusion

In conclusion, we have for the first time monitored the spectral properties of BR monolayer films subjected to external irradiation, resulting in transitions of BR from the **bR** to **Q** states at room temperature. We have shown that the photocycle of monolayer BR films deposited via ESA behave similarly to studies involving 3D volumetric BR samples. In addition, we have found that 755 nm light provides the greatest difference between **bR** and **Q** state absorption spectra with a value of 5.21e-4 at an average surface density of 12.6%. This observation identifies an optimal wavelength to monitor photochromic state changes in BR for use in binary based 2D PBM.

CHAPTER V: Considerations for a Protein Based Disk Storage Device

1. Nano Aperture Waveguides

Nano-aperture waveguides consist of a nanoscale sized aperture on a metal coated source or probe. The aperture is formed via standard nano-fabrication process such

as Focused-Ion-Beam Milling. The ridge waveguide geometry as shown in Figure 27 has been demonstrated to provide superior power transmission of optical sources as compared to circular, square and cross shaped apertures [54]. The ridge waveguide has a greater separation between the cutoff frequency dominant and fist order modes allowing for the transmission of larger wavelength waves through the aperture.

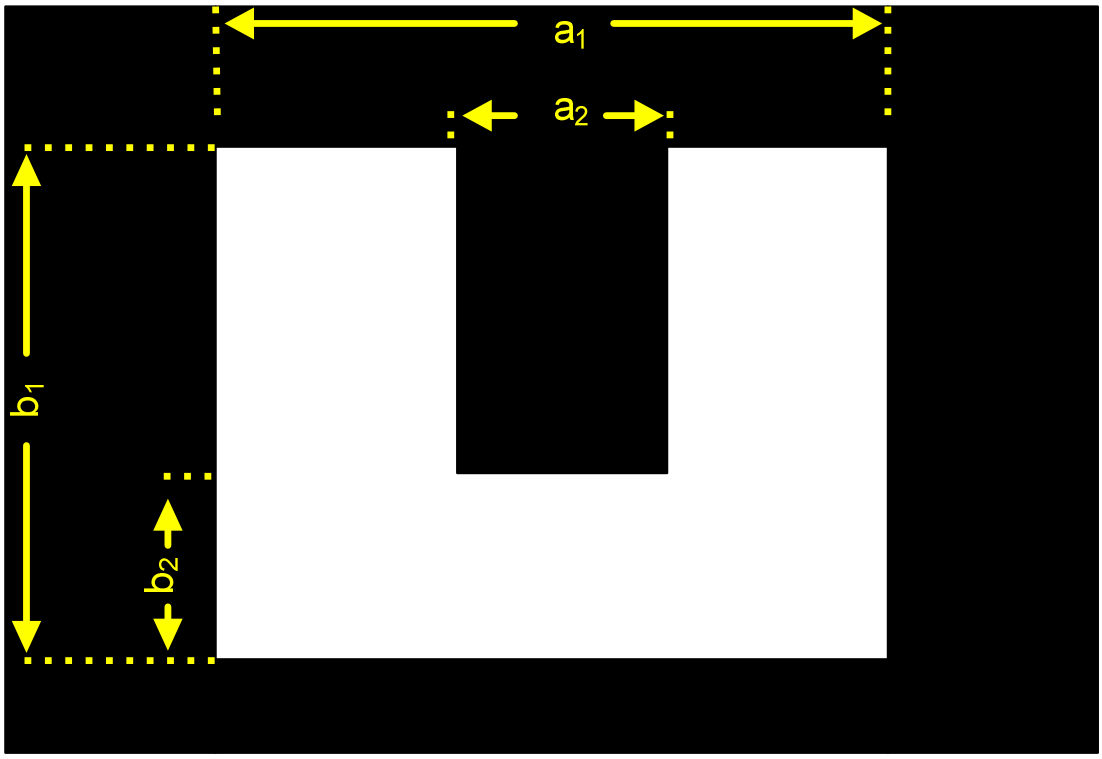

Figure 27: Schematic of a Ridge Waveguide. The width (a2) and height (b2) of the ridge is indicated.

The equivalent circuit of the ridge waveguide is shown in Figure 28. The total waveguide capacitance (C) is indicated and is a combination of the electrostatic (Cs) and discontinuity (Cd) capacitances governed by the following equation:

$$C = C_s + 2*C_d$$

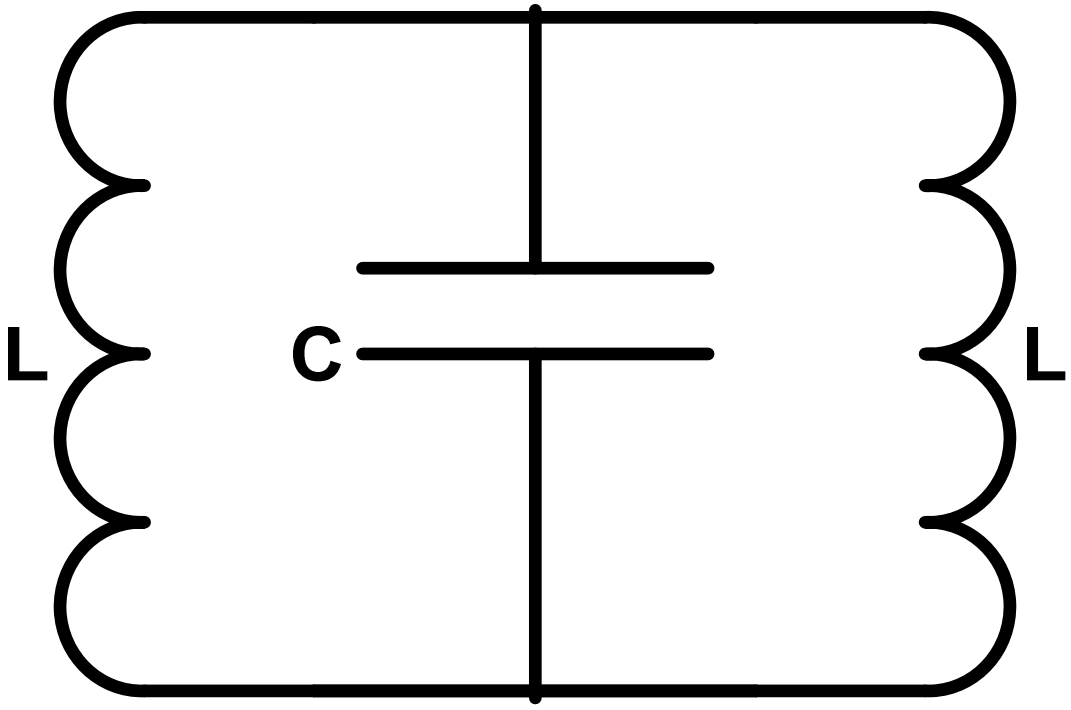

Figure 28: Schematic indicating the equivalent circuit of a Ridge Waveguide consisting of two inductors and a capacitor in parallel.

2. Considerations for the Implementation of 2D Protein Based Memory

a) Introduction

The effect of double erasure on Monolayer Bacteriorhodopsin (BR) protein films after photonic excitation to the ultra stable Q-state is studied. It was found that the pronounced emission of 755nm light occurs only as the protein is made to transition from the Q-state to the ground state via irradiation with blue light. Requirements for the implementation of a next generation Protein-Based Memory (PBM) device utilizing monolayer BR films are considered. The finite element method was used to simulate the optical intensity distribution of nano-aperture waveguides for Red(650nm), Green(510nm) and Blue(475nm) light to analyze the utility of nanoaperture transducers for use in a Protein Based Memory device. The minimum output power required to induce a photochromic transition in BR is calculated to be between 20nW and 27nW on a 30nm spot depending upon the operating wavelength.

As the Superparamagnetic limit promises to stifle further progress in the magnetic disc-based data storage industry, new avenues for technological development in this sector must be pursued to maintain compliance with moor's law [71, 72, and 73]. Currently magnetic storage devices based on perpendicular magnetic recording allow for densities no more than approximately 1TBIT/$in^2$and there has been no consensus as to what new technology will propel future development at a pace which will keep the industry vital in the coming decades [74, 75].

To that end, we propose the development of a bionanotechnological device based on two dimensional (2D) photo-reactive protein films for use as next generation disc-based data storage. The most promising protein for this purpose is Bacteriorhodopsin (BR), the photochemical properties of which have been explained in great detail [25, 26, 30, 32, 33, and 36]. BR possesses within it retinal chromophore, which upon photo-excitation, initiates a proton pumping mechanism commonly described as the photocycle [Figure 1] [33]. This photocycle consists of a series of photostable states some of which are ideally suited for applications in a long term data storage device [45]. BR based 2D protein memory can provide data storage densities in excess of 10TBIT/in^2, while utilizing much of the infrastructure and technology already developed for commercially available hard disc drives [48, 76].

The 2D approach is not to be mistaken for the 3D approach as the 2D method offers significant advantages in regards to the developmental problems faced in making 3D protein-based memory (PBM) devices a reality. These problems include data density limitations resulting from beam steering diffraction effects and dramatic shifts in commercial device implementation methods beyond current industry capability [49, 50, 51, 52, and 53]. Previous studies of BR have focused on large volume samples, presumably under the notion that the 3D implementation would take hold. Herein we explain the promise in utilizing BR in 2D disc based media and the spectral properties of monolayer BR films deposited via Electrostatic Self-

Assembly for use in next generation disc-based data storage devices. In addition, device requirements are proposed related to the throughput of nanoaperture waveguides for the implementation of a PBM device.

b) Experiment

Monolayer BR films were deposited via Electrostatic Self-Assembly (ESA) and the spectra of BR monolayer films were taken on a Cary 5000 Spectrophotometer, ascribing to the methodology presented previously [76]. The spectrophotometer was modified to incorporate an irradiation device consisting of red, blue and green LEDs as shown in Figure 29. This allowed for the excitation of the BR molecule to the desired photostate immediately before each measurement. Simultaneous illumination with Red and Green light excited BR to the Q-state via the short lived O-intermediate state, while Blue light reverted the molecule from Q to the ground state.

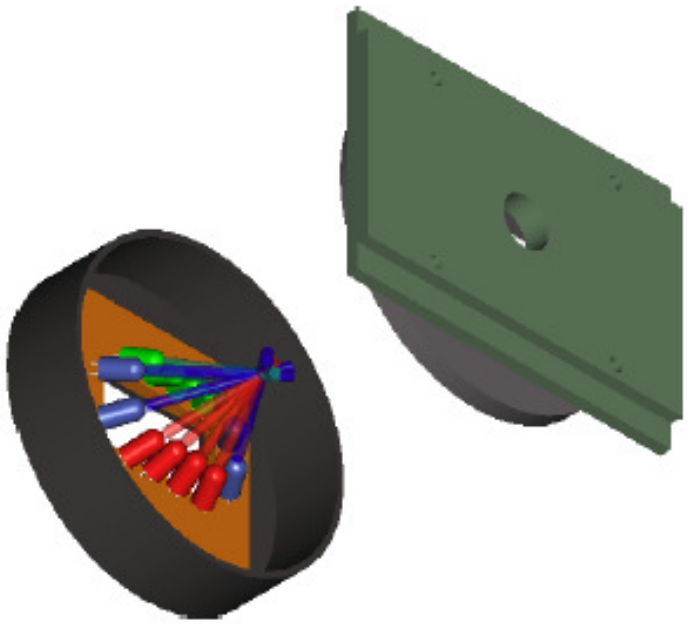

Figure 29: Schematic of LED device used to induce photostate transitions in BR monolayer films.

It was observed that post blue irradiation, ground state BR is made to fluoresce as demonstrated by pronounced negative absorption with maxima occurring at 755nm [Figure 30]. Conversely, BR excited to the Q-state has moderate yet positive absorption, thereby demonstrating large spectral differences between Q-state and ground state in BR monolayer films. Similar measurements on large volume samples show low fluorescence as compared to the absorption of the bulk material [58, 66]. The opposite effect is demonstrated here on 2D BR samples.

Subsequent erasure of the ground state molecule had similar absorption spectra as ground state BR, yielding no pronounced fluorescence as shown in Figure 30. This

eliminates the possibility that the emission of 755nm light was due to excitation of the molecule to resonance and implicates the photocycle as the emission source.

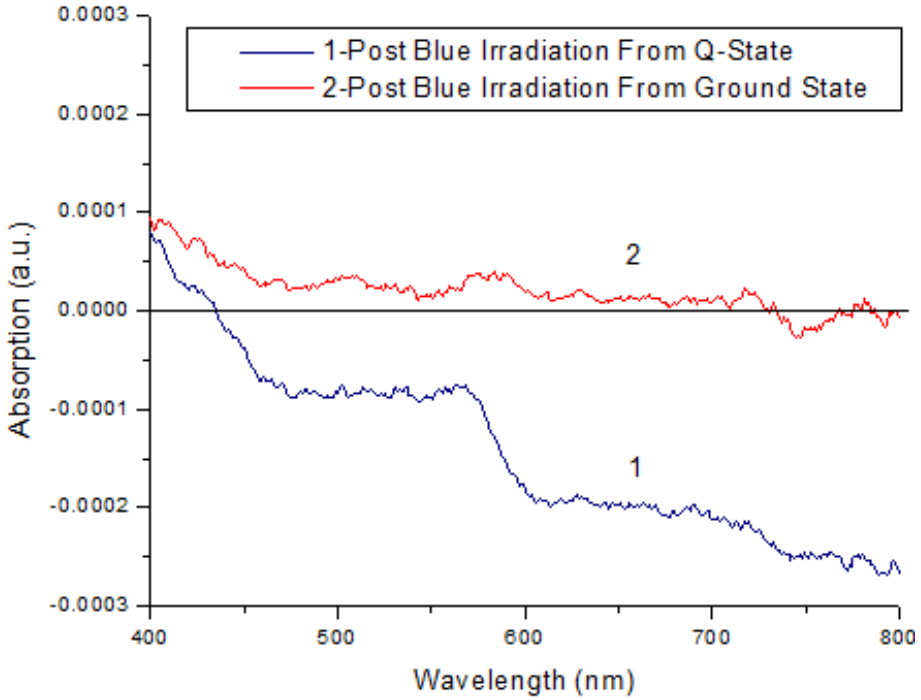

Figure 30: Absorption spectra of BR Monolayer film. 1) after irradiation with blue light from the Q-state and 2) after irradiation with blue light from the ground state.

We propose that the unidirectional proton pumping mechanism, as a process involving the precession of a charged particle throughout the molecule, is suppressed by the influence of the surrounding electrostatic charges inherent to the method of deposition. This leads to the dramatic photoluminescence of BR as the molecule is made to revert to the ground state from the stable Q-state.

The large spectral shift between the Q and ground states, occur when BR is made to transition from the Q-state to the ground state. This affords PBM devices a strong signal response with which to probe the state of 2D media by blue irradiation followed by spectral observation. A PBM device based upon this phenomenon would act first by irradiation with blue light. Strong fluorescence in the protein indicates that BR was in the Q-state or binary 1, and the bit can be re-written. No fluorescence indicates ground state BR, or binary 0. Thus, this observation imposes the requirement that PBM devices based on BR monolayer films incorporate a two-step read process in which the bit is first irradiated with blue light, then fluorescence at 755nm if any, is measured and finally the data is re-written if necessary [Figures 31 and 32].

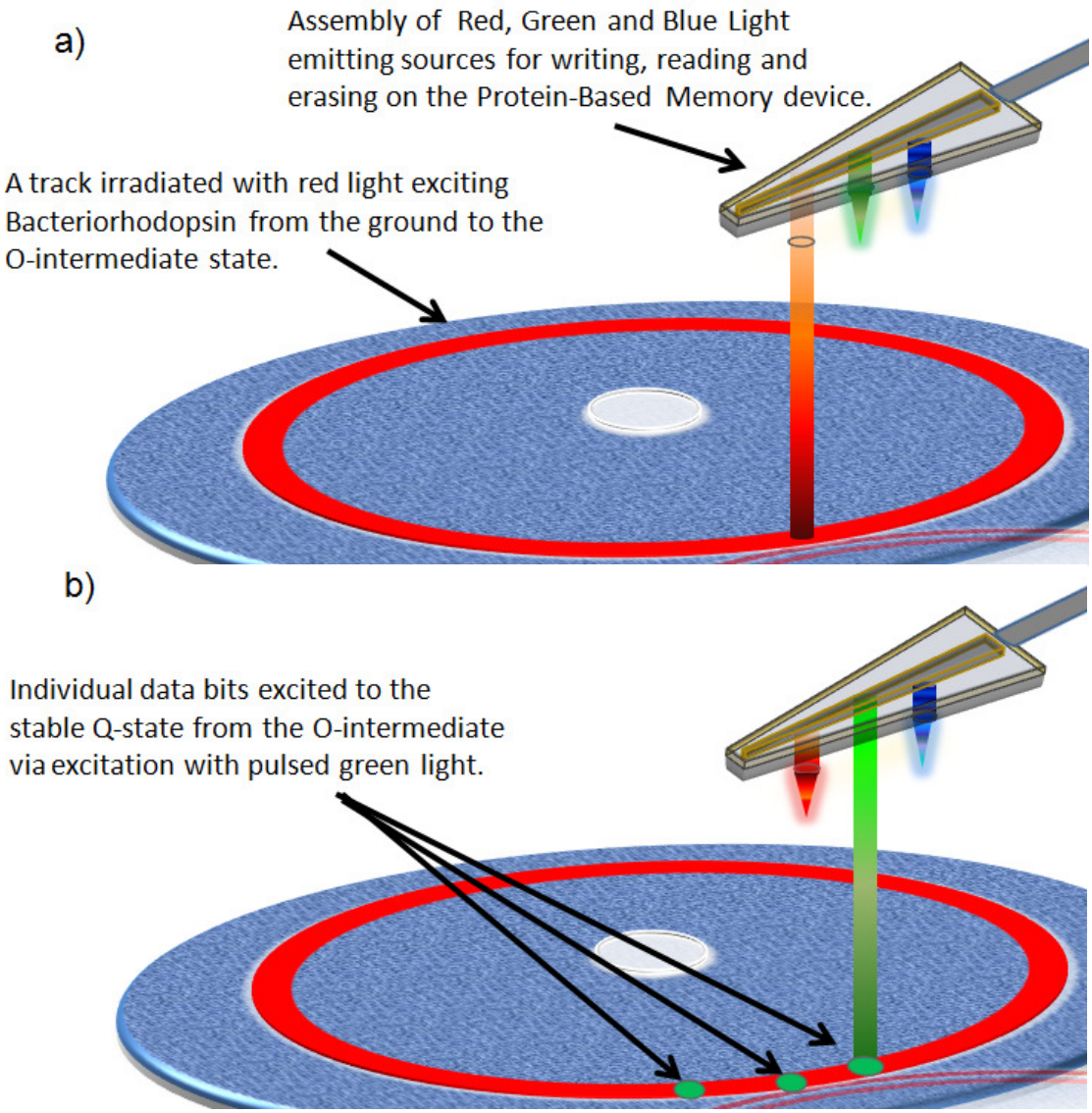

Figure 31: Protein-Based Memory Data Writing Schematic. a) Irradiation with Red light excites the protein data track to the O-intermediate state from the ground state. b) Green light induces a transition to the Q-state or binary 1.

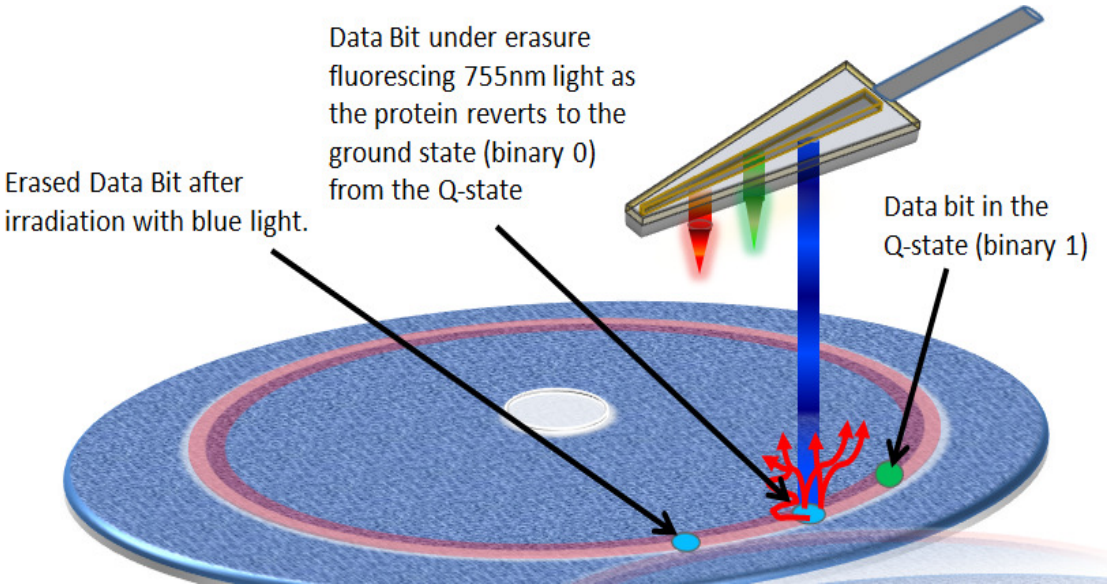

Figure 32: Protein Based Memory Data Erasure and Read Mechanism Schematic: Irradiation with Blue light reverts the protein to the ground state or binary 0, resulting in pronounced fluorescence of the media.

Another possible method for use as the read/write process of a PBM device is to exploit the difference in absorption of red light between Q-state and ground state BR [48]. Q-state BR does not interact with red light. Ground state BR absorbs red light inducing a transition of the protein to the O-intermediate state where, unless green light is used to transition the protein to the Q-state, the protein reverts to the ground state. Determination of the state of the protein with this method depends upon the absorption of the BR film. While this method remains an option, the fluorescence based method provides a more pronounced signal response for device applications.

Recent studies into nano-aperture optical transducers have indicated the optimal waveguide geometry with which to provide sufficient output power for use in Heat Assisted Magnetic Recording systems [54]. The authors were able to produce a device which delivers 100nW of power to a 30nm spot on the media's surface. The high quantum efficiency of BR, ~66%, is such that only two photons are required to ensure a photochromic transition between states within the photocycle [77]. The power delivered to the media's surface is related to the sum of the Energy of all photons incident on the media, as the energy of photons are quantized. The total energy delivered in a two photon system is:

$$\text{E = Power*time} = \frac{nhc}{\lambda}$$

- h is Planks constant,
- c is the speed of light,
- n is the quantity of photons and
- λ is the photons wavelength.

Here we take the time to be 7ns, which was the time used to establish the quantum efficiency of BR [77]. This provides the requirement that 0.09nW for Red light, 0.11nW for Green light and 0.12nW for Blue light be delivered to the sample through the waveguide on a 2nm spot, which is the dimension of a single PM sheet as deposited via ESA. By comparison this equates to 20nW, 25nW and 27nW of

power at the sample surface for Red, Green and Blue light respectively for a 30nm spot, far less than has already been demonstrated experimentally.

c) 3D Finite Element Analysis

The 3D finite element method was used to model the optical intensity distribution of an aluminum coated ridge waveguide for Red(650nm), Green(510nm) and Blue(475nm) light [Figure 33]. The waveguide dimensions were taken from literature [54]. The results are presented in Figures 34-36. It was observed that the optical intensity distribution has insufficient confinement for 475nm light, while the geometry is optimal for 510nm light. Further research is required to determine a suitable waveguide for use with blue light. Unless a single nano-aperture waveguide design can be obtained for use with Red, Green and Blue light, a two aperture device implementation may be necessary.

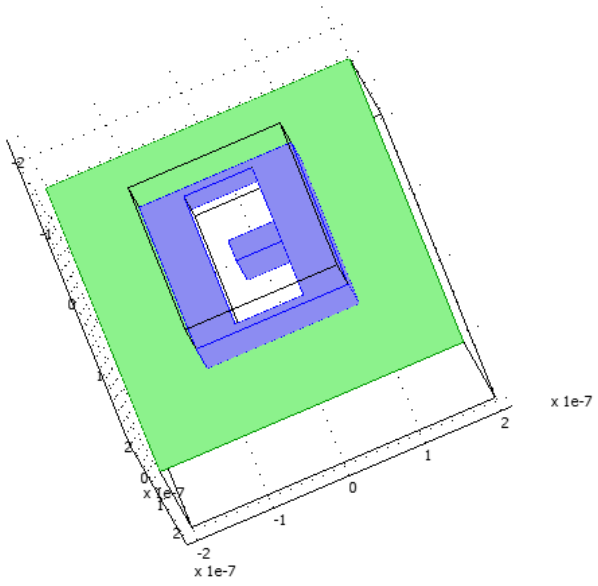

Figure 33: A Ridge Waveguide oriented perpendicularly to the protein media layer.

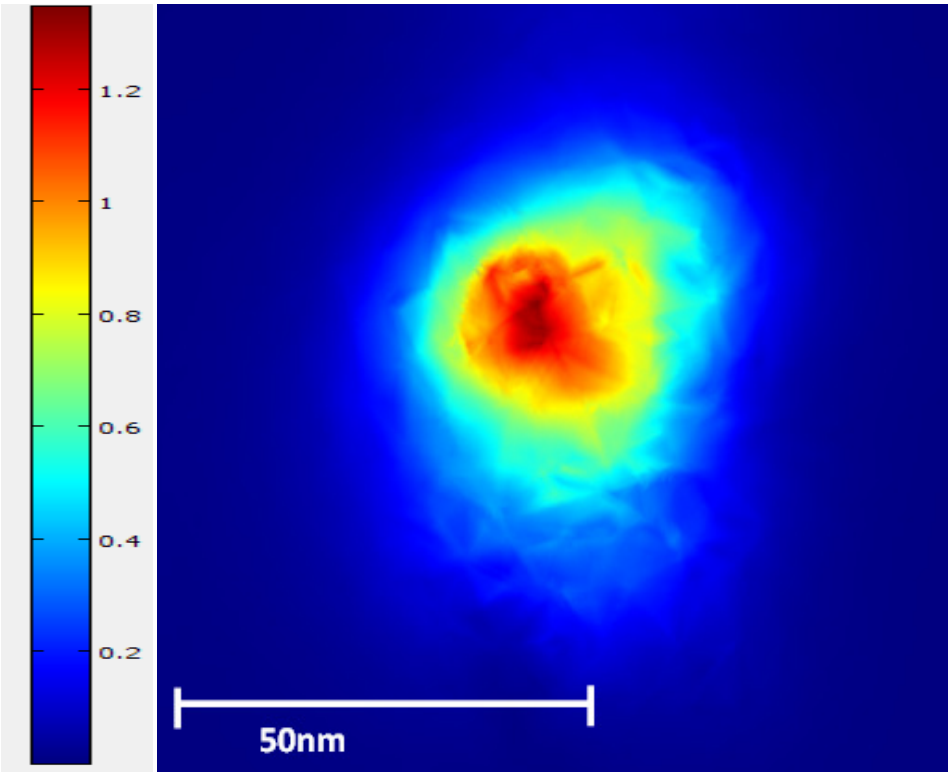

Figure 34: Optical intensity of 650nm light through a Ridge Waveguide as modeled by the 3D Finite Element Method.

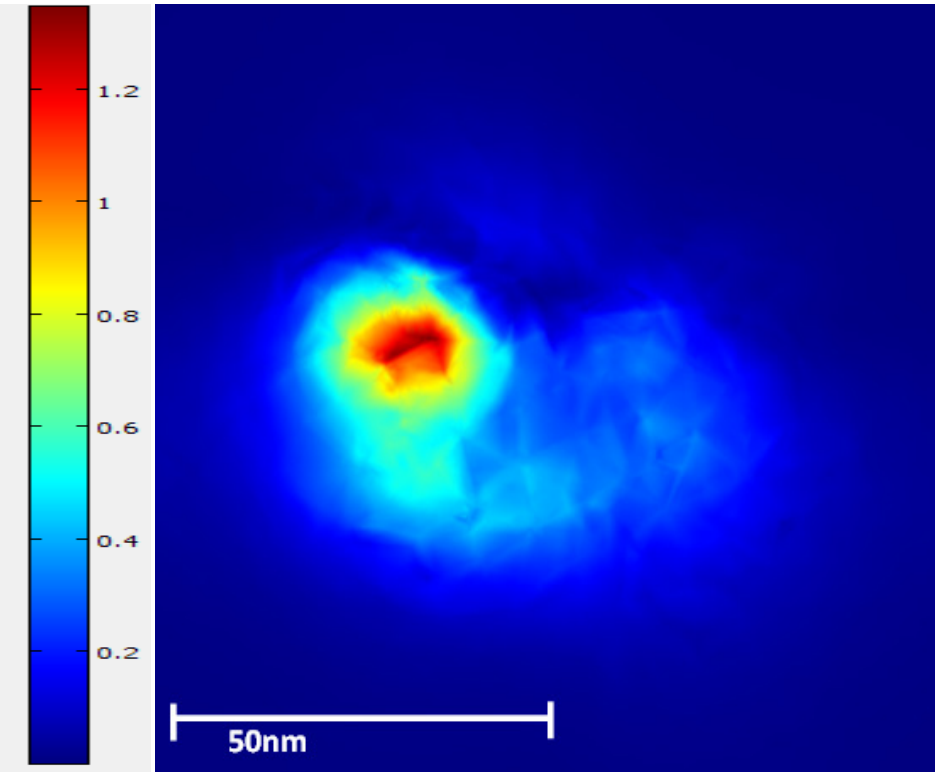

Figure 35: Optical intensity of 510nm light through a Ridge Waveguide as modeled by the 3D Finite Element Method.

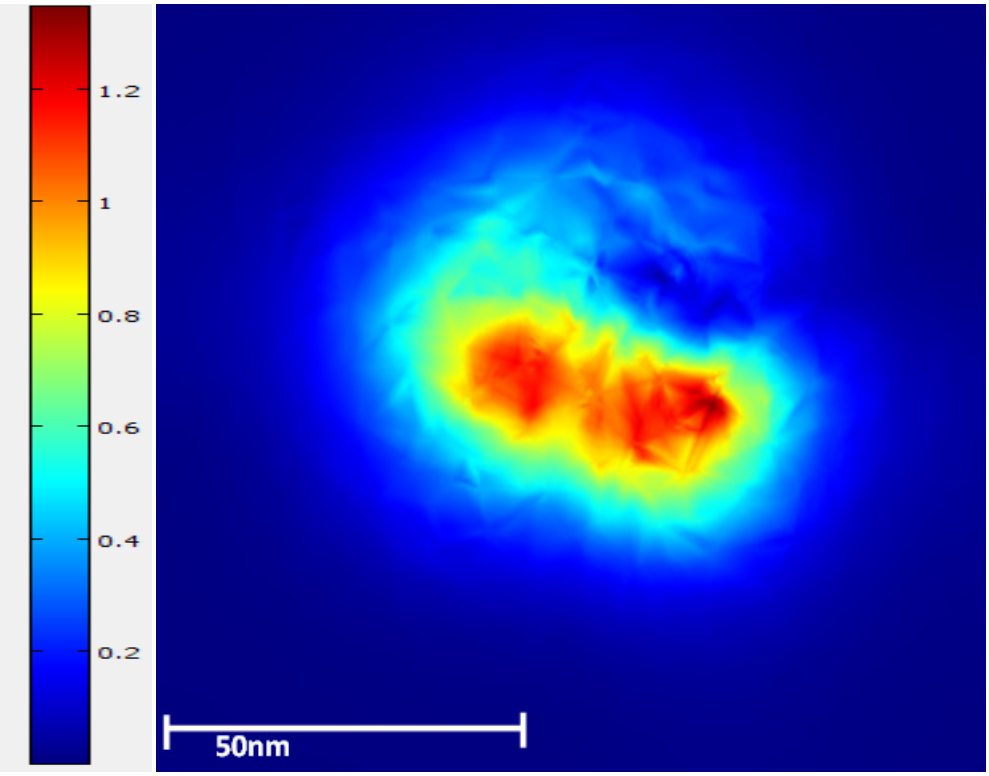

Figure 36: Optical intensity of 475nm light through a Ridge Waveguide as modeled by the 3D Finite Element Method.

d) Conclusion

In conclusion, the photoresponse of monolayer Bacteriorhodopsin in the form of pronounced fluorescence of the media as the protein is made to revert to the ground state from the stable Q-state is demonstrated. In addition, we propose a two-step read process as a means of determining the photostate of the protein media. The minimum power required to induce a photochromic transition was calculated to be 20nW, 25nW and 27nW for Red, Green and Blue light respectively on a 30nm spot. The 3D finite element method was used to model the output power of nano-

aperture ridge waveguides for Red(650nm), Green(510nm) and Blue(475nm) light for use in a Protein Based Memory device.

REFERENCES

1. E. Daniel, C. Mee, and M. Clark, Magnetic Recording The First 100 Years, pp.270-299, IEEE Press (**1999**)

2. S. H. Charap, P.-L. Lu, Y. He. Thermal Stability of Recorded Information at High Densities. *IEEE Trans. Magn*., **33** (1), 978-83 (**1997**)

3. Zhu, J. -G., IEEE Trans. Magn. (**1992**) 27, 5040

4. 4 Zhu, J. -G., and Bertram, H. N., J. Appl. Phys. (**1988**) 63, 3248

5. P. Herget, T. Rausch, A. C. Shiela, D. D. Stancil, T. E. Schlesinger, J.-G. Zhu, and J. A. Bain. Mark shapes inybrid recording. Appl. Phys. Lett. **80** (11), 1835-7 (**2002**)

6. M. Albrecht, C. T. Rettner, A. Moser, M. E. Best, and B. D. Terris. Recording performance of high-density patterned perpendicular media. *Appl. Phys. Lett*. **81** (15), 2875-7 (**2002**)

7. C. Chappert, H. Bernas, J. Ferré, V. Kottler, J.-P. Jamet, Y. Chen, E. Cambril, T. Devolder, F. Rousseaux, V. Mathet, and H. Launois, Science ***280**, 1919 (**1998**)*

8. T. McDaniel, W. Challener. Issues in heat-assisted perpendicular recording. *IEEE Trans. Magn.* **39** (4), 1972-9 (**2003**)

9. D. Weller and A. Moser, IEEE Trans. Magn*. **35**, 4423 (**1999**)*

10. R. L. White, R. M. H. New, and R. F. W. Pease, IEEE Trans. Magn. ***33**, 990 (**1997**)*

11. C. A. Ross, H. I. Smith, T. Savas, M. Schattenburg, M. Farhoud, M. Hwang, M. Walsh, M. C. Abraham, and R. J. Ram, J. Vac. Sci. Technol. *B **17**, 3168 (**1999**)*

12. H. F. Hamann, Y. C. Martin, and H. K. Wickramasighe. Thermally assisted recording beyond traditional limits*. Appl. Phys. Lett*. **84** (5), 810 (**2004**)

13. P. B. Fischer and S. Y. Chou. 10 nm Electron Beam Lithography and Sub-50 nm Overlay Using A Modified Electron Microscope. *Appl. Phys. Lett*. **62**, 2989 (**1993**)

14. S. Khizroev, Y. Liu, K. Mountfield, M. Kryder, D. Litvinov. Physics of perpendicular magnetic recording: writing process. JMMM **246** (1-2), 335-44 (**2002**)

15. S. Khizroev and D. Litvinov**,** *Perpendicular Magnetic Recording*, Kluwer Academic Publishers, **2004**; ISBN 1-4020-2662-5

16. S. Iwasaki and Y. Nakamura. An analysis for the magnetization mode for high density magnetic recording. IEEE Trans. Magn., **13**, 1272 (**1977**)

17. S. Hunter, F. Kiamilev, S. Esener, D. Parthenopoulos, P.M. Rentzepis, *Appl. Opt.* **29**, 2058 (**1990**)

18. R.R. Birge, *Sci. Am.* **82**, 348 (**1994**)

19. R.E. Armstrong, J.B. Warner. Biology and the Battlefield. *Defense Horizons 25* (Center for Technology and National Security Policy, National Defense University, Washington, DC, March **2003**)

20. D. Oesterhelt, W. Stoeckenius, *Proc. Natl. Acad. Sci. U.S.A.* **70**, 2853 (**1973**)

21. T. Tsujioka, F. Tatezono, T. Harado, K. Kuroki, M. Irie, *Jpn. J. Appl. Phys.* **33**, 5788 (**1994**)

22. R. Thoma, N. Hampp, *Opt. Lett.* **17** (16), 1158 (**1992**)

23. R.R. Birge, U.S. Patent 5,559,732 (**1994**)

24. J.A. Stuart, D.L. Marcy, K.J. Wise, R.R. Birge, *Synth. Met.* **127**, 3 (**2002**)

25. D. Osterhelt and W. Stockenius, Functions of a new photoreceptor membrane. Proc. Natl. Acad. Sci. USA. vol. 70, 2853-2857 (**1973**)

26. H. Luecke. Atomic resolution structures of bacteriorhodopsin photocycle intermediates: the role of discrete water molecules in the function of this light-driven ion pump. Biochim. Biophys. Acta. vol. 1460, 133–156 (**2000**)

27. T. Oka, K. Inoue, M. Kataoka, Y. Yagi, *Biophys. J.* **88** (1), 436 (**2005**)

28. N. Grigorieff, T.A. Ceska, K.H. Downing, J.M. Baldwin, R. Henderson, *J. Mol. Biol.* **259**, 393 (**1996**)

29. R. Henderson, G.F.X. Schertler, *Philos. Trans. R. Soc. London, Ser. B* **326** (1236), 379 (**1990**)

30. H. Luecke, H.T. Richter, and J.K. Lanyi. Proton Transfer Pathways in Bacteriorhodopsin at 2.3 Angstrom Resolution. Science. vol. 280, 1934 (**1998**)

31. E.G. Pebay-Peyroula, G. Rummel, J.P. Rosenbusch, E.M. Landau, *Science* **277**, 1676 (**1997**)

32. N. Gillespie, K. Wise, L. Ren, J. Stuart, D. Marcy, J.Hillebrecht, Q. Li, L. Ramos, K. Jordan, S. Fyvie, and R. Birge, Characterization of the Branched-Photocycle

Intermediates P and Q of Bacteriorhodopsin. J. Phys. Chem. B. vol. 106, 13352-13361 (**2002**)

33. Popp, M. Wolperdinger, N. Hampp, C. Brauchle, and D. Oesterhelt. Photochemical conversion of the O-intermediate to 9-cis-retinal-containing products in bacteriorhodopsin films. Biophysical Journal. vol. 65 (4), 1449-1459 (**1993**)

34. B. Schobert, J. Cupp-Vickery, V. Hornak, S. Smith and J. Lanyi. Crystallographic structure of the K intermediate of bacteriorhodopsin: conservation of free energy after photoisomerization of the retinal. J. Mol. Biol. vol. 321, 715–726 (**2002**)

35. N. Gillespie, L. Ren, L. Ramos, H. Daniell, D. Dews, K. Utzat, J. Stuart, C. Buck, and R. Birge. Characterization and Photochemistry of 13-Desmethyl Bacteriorhodopsin. J. Phys. Chem. B. vol. 109 (33), 16142-16152 (**2005**)

36. G. Varo, J.K. Lanyi, *Biochemistry* **30** (20), 5016 (**1991**)

37. M. Wolperdinger, N. Hampp, *Biophys. Chem.* **56**, 189 (**1995**)

38. S.P. Balashov, *Isr. J. Chem.* **35**, 415 (**1995**)

39. T. Rink, M. Pfeiffer, D. Osterhelt, K. Gerwert, H.-J. Steinhoff, *Biophys. J.* **78**, 1519 (**2000**)

40. A. Popp, M. Wolperdinger, N. Hampp, C. Brauchle, D. Oesterhelt, *Biophys. J.* **65**, 1449 (**1993**)

41. E.M. Landau, J.P. Rosenbusch, *Proc. Natl. Acad. Sci. U.S.A.* **93**, 14532 (**1996**)

42. A. Campion, J. Terner, M.A. El-Sayed, *Nature* **256**, 659 (**1977**)

43. G. Varo, J.K. Lanyi, *Biochemistry* **30**, 5008 (**1991**)

44. N. Hampp. Bacteriorhodopsin: mutating a biomaterial into an optoelectronic material. Appl. Microbiol. Biotechnol. vol. 53, 633 (**2000**)

45. R. Birge, N. Gillespie, E. Izaguirre, A. Kusnetzow, A. Lawrence, D. Singh, Q. Song, E. Schmidt, J. Stuart, S. Seetharaman, and K. Wise. Biomolecular Electronics: Protein-Based Associative Processors and Volumetric Memories. J. Phys. Chem. B. vol. 103, 10746-10766 (**1999**)

46. A. Miniewicz, V. Renugopalakrishnan, in *Bionanotechnology : Proteins to Nanodevices,* V. Renugopalakrishnan, R.V. Lewis, Eds. (Springer, New York, **2006**)

47. J.L. Spudich, *Science* **288** (5470), 1358 (**2000**)

48. S. Khizroev, R. Ikkawi, N. Amos, R. Chomko, V. Renugopalakrishnan, R. Haddon, and D. Litvinov. Protein-Based Disk Recording at Arial Densities beyond 10 Terabits/in^2. MRS Bulletin. vol. 33, 1-8 (**2008**)

49. Z. Chen, D. Govender, R. Gross, and R. Birge, Advances in protein-based three-dimensional optical memories. BioSystems. vol. 35, 145-151 (**1995**)

50. J. Stuart, D. Marcy, K. Wise and R. Birge, Volumetric optical memory based on bacteriorhodopsin. Synthetic Metals. vol. 127, 3–15 (**2002**)

51. R. Birge. Protein-based optical computing and memories. Computer. vol. 25 (11), 56-67 (**1992**)

52. R. Birge, R.B. Gross, M.B. Masthay, J.A. Stuart, J.R. Tallent and C.F. Zhang. Nonlinear optical properties of bacteriorhodopsin and protein based two-photon three-dimensional memories. Mol. Cryst. Liq. Sci. Technol. Sec. B. Nonlin. Opt. vol. 3, 133-147 (**1992**)

53. S. Rajasekaran, V. Kumar, S. Sahni, R. Birge. Efficient algorithms for protein-based associative processors and volumetric memories. Proceedings of the 8th IEEE Conference on Nanotechnology, (**2008**) pp. 397-400 Arlington, TX.

54. R. Ikkawi, N. Amos, A. Krichevsky, R. Chomko, D. Litvinov and S. Khizroev. Nanolasers to enable data storage beyond 10 Tbit/in.^{2} Appl. Phys. Lett. vol. 91, 153115 (**2007**)

55. J. He, L. Samuelson, L. Li, J. Kumar, and S. K. Tripathy. Oriented Bacteriorhodopsin/Polycation Multilayers by Electrostatice Layer-by-Layer Assembly. Langmuir. vol. 14 (7), 1674-1679(**1998**)

56. P. Bertrand, A. Jonas, A. Laschewsky, and R. Legras. Ultrathin polymer coatings by complexation of polyelectrolytes at interfaces: suitable materials, structure and properties. *Macromol. Rapid Commun.* vol. 21, 319-348 (**2000**)

57. Y. Shen, C. R. Safinya, K. S. Liang, A. F. Ruppert, and K. J. Rothschild. Stabilization of the membrane protein bacteriorhodopsin to 140 °C in two-dimensional films. Nature vol. 366, 48-50 (**1993**)

58. A. Andreeva, V. Kolev, and T. Lazarova. Fluorescence spectroscopy of bacteriorhodopsin at room temperature. Proc. SPIE. vol. 3573, 359-362 (**1998**)

59. A. Lewis, J. P. Spoonhower, and G. J. Perreault. Observation of light emission from a rhodopsin. Nature. vol. 260, 675-678 (**1976**)

60. R. Sarpeshkar, T. Delbruck, C.A. Mead, *IEEE Circuits Devices Mag.* 23 (November **1993**)

61. R. Govindjee, B. Becher, and T. S. Ebrey. The fluorescence from chromophore of the BR protein. Biophys. J. vol. 22, 67-77 (**1978**)

62. V. A. Sineshchekov and F. F. Litvin. Luminescence of bacteriorhodopsin from Halobacterium halobium and its connection with the photochemical conversions of the chromophore. Biochim. Biophys. Acta. vol. 462, 450-466 (**1977**)

63. N.B. Gillespie, L. Ren, L. Ramos, H. Daniel, D. Dews, K.A. Utzat, J.A. Stuart, C.H. Buck, R. Birge, *J. Phys. Chem. B* **109** (33), 16142 (**2005**)

64. A. N. Kriebel, T. Gi1LA-bRo, and U. P. Wild. A low temperature investigation of the intermediates of the photocycle of light-adapted bacteriorhodopsin. Optical absorption and fluorescence measurements. Biochim. Biophys. Acta. vol. 546, 106-120 (**1979**)

65. Y. Yokoyama, M. Sonoyama, S. Mitaku, *J. Biochem.* **131**, 785 (**2002**)

66. H. Ohtani, Y. Tsukamoto, Y. Sakoda, and H. Hainaguchi. Fluorescence spectra of bacteriorhodopsin and the intermediates O and Q at room temperature. FEBS Lett. vol. 359(1), 65-68 (**1995**)

67. T. Tsujioka, M. Irie, *Appl. Opt.* **37** (20), 4419 (**1998**)

68. A. Lewis, and G.J.Perreault. Emission spectroscopy of rhodopsin and bacterirhodopsin. Methods in Enzymology. vol. 88, 217-229 (**1982**)

69. T. Gillbro, A. N. Kriebel, and U. P. Wild. On the origin of the red emission of light adapted BR of Halobacterium halobium. FEBS Lett. vol. 78(1), 57-60 (**1977**)

70. G. H. Atkinson, D. Blanchard, H. Lemaire, T. L. Brack, and H. Hayashi. Picosecond time-resolved fluorescence spectroscopy of K-590 in the bacteriorhodopsin photocycles. Biophys. J. vol. 55, 263-274 (**1989**)

71. R. Rottmayer, S. Batra, D. Buechel, W. Challener, J. Hohlfeld, Y. Kubota, L. Li, B. Lu, C. Mihalcea, K. Mountfield, K. Pelhos, C. Peng, T. Rausch, M. Seigler, D. Weller, and X. Yang. Heat-assisted magnetic recording. IEEE Trans. Mag. vol.42, 2417–2421 (**2006**)

72. P. L. Lu and S. H. Charap. Magnetic viscosity in high-density recording. J. Appl. Phys. vol. 75, 5768-5770 (**1994**)

73. D. Weller and A. Moser, Thermal effect limits in ultrahigh density magnetic recording, IEEE Trans. Magn. vol. 35, 4423–4439 (**1999**)

74. S. I. Iwasaki and J. Hokkyo. Perpendicular Magnetic Recording. (IOS, Amsterdam, **1991**)

75. M. Mallary, A. Torabi, and M. Benakli. One terabit per square inch perpendicular recording conceptual design. IEEE Trans. Magn. vol. 38, 1719–1724 (**2002**)

76. M.Hudgins, J. Butler, R. Fernandez, F. Gertz, M.Ranagan, R.Birge, R. Haddon, and S. Khizroev. Photo-response of Electrostatically Deposited Bacteriorhodopsin Monolayer Films for Protein-Based Disk Recording Beyond 10 Tbi/in.^{2} J. Nanoelectron. Optoelectron. (In Press)

77. R. Govindjee, S. P. Balashov, and T. G. Ebrey. Quantum efficiency of the photochemical cycle of bacteriorhodopsin. Biophys. J. vol. 58, 597-608 (**1990**)

PUBLICATION LIST

1. R. Fernandez, N. Amos, C. Zhang, M. Hudgins, and S. Khizroev. Microstructural enhancement of high coercivity L10 FePt films for next-generation magnetic recording media. J. Nanoscience and Nanotechnology (In Press)

2. M.Hudgins, J. Butler, R. Fernandez, F. Gertz, M.Ranagan, R.Birge, R. Haddon, and S. Khizroev. Photo-response of Electrostatically Deposited Bacteriorhodopsin Monolayer Films for Protein-Based Disk Recording Beyond 10 Tbi/in.^{2} J. Nanoelectron. Optoelectron. (In Press)

3. M.Hudgins and S. Khizroev. Considerations for the Implementation of 2D Protein Based Memory. J. Nanoscience and Nanotechnology (In Press)